

1 **An eQTL-based Approach Reveals Candidate L1 Transcriptional Regulators in**
2 **Lymphoblastoid Cells**

3 Juan I. Bravo^{1,2}, Chanelle R. Mizrahi^{1,3}, Seungsoo Kim⁴, Lucia Zhang^{1,5}, Yousin Suh^{4,6},
4 B er enice A. Benayoun^{1,7,8,9,10}

5 ¹ Leonard Davis School of Gerontology, University of Southern California, Los Angeles,
6 CA 90089, USA.

7 ² Graduate program in the Biology of Aging, University of Southern California, Los
8 Angeles, CA 90089, USA.

9 ³ USC Gerontology Enriching MSTEM to Enhance Diversity in Aging Program,
10 University of Southern California, Los Angeles, CA 90089, USA.

11 ⁴ Department of Obstetrics and Gynecology, Columbia University Irving Medical Center,
12 New York, NY 10032, USA.

13 ⁵ Quantitative and Computational Biology Department, USC Dornsife College of Letters,
14 Arts and Sciences, Los Angeles, CA 90089, USA.

15 ⁶ Department of Genetics and Development, Columbia University Irving Medical Center,
16 New York, NY 10032, USA.

17 ⁷ Molecular and Computational Biology Department, USC Dornsife College of Letters,
18 Arts and Sciences, Los Angeles, CA 90089, USA.

19 ⁸ Biochemistry and Molecular Medicine Department, USC Keck School of Medicine, Los
20 Angeles, CA 90089, USA.

21 ⁹ USC Norris Comprehensive Cancer Center, Epigenetics and Gene Regulation, Los
22 Angeles, CA 90089, USA.

23 ¹⁰ USC Stem Cell Initiative, Los Angeles, CA 90089, USA.

24

25

26 **Abstract**

27 Long interspersed element 1 (L1) are a family of autonomous, actively mobile
28 transposons that occupy ~17% of the human genome. The pleiotropic effects L1
29 induces in host cells (promoting genome instability, inflammation, or cellular
30 senescence) are established, and L1's associations with aging and aging diseases are
31 widely recognized. However, because of the cell type-specific nature of transposon
32 control, the catalogue of L1 regulators remains incomplete. Here, we employ an eQTL
33 approach leveraging transcriptomic and genomic data from the GEUVADIS and
34 1000Genomes projects to computationally identify new candidate regulators of L1
35 expression in lymphoblastoid cell lines. To cement the role of candidate genes in L1
36 regulation, we experimentally modulate the levels of top candidates *in vitro*, including
37 *IL16*, *STARD5*, *HSDB17B12*, and *RNF5*, and assess changes in TE family expression
38 by Gene Set Enrichment Analysis (GSEA). Remarkably, we observe subtle but
39 widespread upregulation of TE family expression following *IL16* and *STARD5*
40 overexpression. Moreover, a short-term 24-hour exposure to recombinant human IL16
41 was sufficient to transiently induce subtle but widespread upregulation of *L1*
42 subfamilies. Finally, we find that many L1 expression-associated genetic variants are
43 co-associated with aging traits across genome-wide association study databases. Our
44 results expand the catalogue of genes implicated in L1 transcriptional control and
45 further suggest that L1 contributes to aging processes. Given the ever-increasing
46 availability of paired genomic and transcriptomic data, we anticipate this new approach
47 to be a starting point for more comprehensive computational scans for transposon
48 transcriptional regulators.

49

50 Introduction

51 Transposable elements (TEs) constitute ~45% of the human genome ¹. Among
52 these, the long interspersed element-1 (LINE-1 or L1) family of transposons is the most
53 abundant, accounting for ~16-17% ^{1,2}, and remains autonomously mobile, with humans
54 harboring an estimated 80-100 retrotransposition-competent L1 copies ³. These
55 retrotransposition competent L1s belong to evolutionarily younger L1PA and L1Hs
56 subfamilies, are ~6 kilobases long, carry an internal promoter in their 5'-untranslated
57 region (UTR), and encode two proteins — L1ORF1p and L1ORF2p — that are
58 necessary for transposition ⁴. The remaining ~500,000 copies are non-autonomous or
59 immobile because of the presence of inactivating mutations or truncations ¹ and include
60 L1 subfamilies of all evolutionary ages, including the evolutionarily older L1P and L1M
61 subfamilies. Though not all copies are transposition competent, L1s can nevertheless
62 contribute to aspects of aging ^{5,6} and aging-associated diseases ⁷⁻¹⁰.

63 Though mechanistic studies characterizing the role of L1 in aging and aging-
64 conditions are limited, its effects are clearly pleiotropic. L1 can contribute to genome
65 instability via insertional mutagenesis, leading to an expansion of copy number with
66 organismal aging ¹¹ and during cellular senescence ¹². L1 can also play a contributing
67 role in shaping inflammatory and cellular senescence phenotypes. The secretion of a
68 panoply of pro-inflammatory factors is a hallmark of cell senescence, called the
69 senescence associated secretory phenotype (SASP) ¹³. Importantly, the SASP is
70 believed to stimulate the innate immune system and contribute to chronic, low-grade,
71 sterile inflammation with age, a phenomenon referred to as “inflamm-aging” ^{13,14}. During
72 deep senescence, L1 are transcriptionally de-repressed and consequently generate
73 cytosolic DNA that initiates an immune response consisting of the production and
74 secretion of pro-inflammatory interferons ¹⁵. Finally, L1 is causally implicated in aging-
75 associated diseases, including cancer. L1 may contribute to cancer by (i) serving as a
76 source for chromosomal rearrangements that can lead to tumor-suppressor genes
77 deletion ¹⁶ or (ii) introducing its active promoter next to normally silenced oncogenes ¹⁷.
78 Thus, because of the pathological effects L1 can have on hosts, it is critical that hosts
79 maintain precise control over L1 activity.

80 Eukaryotic hosts have evolved several pre- and post-transcriptional mechanisms
81 for regulating TEs ^{18,19}. Nevertheless, our knowledge of regulatory genes remains
82 incomplete because of cell type-specific regulation and the complexity of methods
83 required to identify regulators. Indeed, one clustered regularly interspaced short
84 palindromic repeats (CRISPR) screen in two cancer cell lines for regulators of L1
85 transposition identified >150 genes involved in diverse biological functions ²⁰ (e.g.
86 chromatin regulation, DNA replication, and DNA repair). However, only about ~36% of
87 the genes identified in the primary screen exerted the same effects in both cell lines ²⁰,
88 highlighting the potentially cell type-specific nature of L1 control. Moreover, given the
89 complexities of *in vitro* screens, especially in non-standard cell lines or primary cells, *in*
90 *silico* screens for L1 regulators may facilitate the task of identifying and cataloguing
91 candidate regulators across cell and tissue types. One such attempt was made by
92 generating gene-TE co-expression networks from RNA sequencing (RNA-seq) data
93 generated from multiple tissue types of cancerous origin ²¹. Although co-expression
94 modules with known TE regulatory functions, such as interferon signaling, were
95 correlated with TE modules, it is unclear whether other modules may harbor as of now
96 uncharacterized TE-regulating properties, since no validation experiments were carried
97 out. Additionally, this co-expression approach is limited, as no mechanistic directionality
98 can be assigned between associated gene and TE clusters, complicating the
99 prioritization of candidate regulatory genes for validation. Thus, there is a need for the
100 incorporation of novel “omic” approaches to tackle this problem. Deciphering the
101 machinery that controls TE activity in healthy somatic cells will be crucial, in order to
102 identify checkpoints lost in diseased cells.

103 The 1000Genomes Project and GEUVADIS Consortium provide a rich set of
104 genomic resources to explore the mechanisms of human TE regulation *in silico*. Indeed,
105 the 1000Genomes project generated a huge collection of genomic data from thousands
106 of human subjects across the world, including single nucleotide variant (SNV) and
107 structural variant (SV) data ^{22,23}. To accomplish this, the project relied on lymphoblastoid
108 cell lines (LCLs), which are generated by infecting resting B-cells in peripheral blood
109 with Epstein-Barr virus (EBV). Several properties make them advantageous for use in
110 large-scale projects (e.g. they can be generated relatively uninvassively, provide a

111 means of obtaining an unlimited amount of a subject's DNA and other biomolecules,
112 and can serve as an *in vitro* model for studying the effects of genetic variation with
113 phenotypes of interest) ^{24,25}. Indeed, the GEUVADIS Consortium generated
114 transcriptomic data for a subset of subjects sampled by the 1000Genomes Project, and
115 used their genomic data to define the effects genetic variation on gene expression ²⁶.
116 Together, these resources provide a useful toolkit for investigating the genetic
117 regulation of TEs, generally, and L1, specifically.

118 In this study, we (i) develop a pipeline to identify novel candidate regulators of L1
119 expression in lymphoblastoid cell lines, (ii) provide experimental evidence for the
120 involvement of top candidates in L1 expression control, and (iii) expand and reinforce
121 the catalogue of diseases linked to L1.

122

123

124 **Results**

125 *In silico scanning for L1 subfamily candidate regulators by eQTL analysis*

126 To identify new candidate regulators of L1 transcription, we decided to leverage
127 publicly available human “omic” datasets with both genetic and transcriptomic
128 information. For this analysis, we focused on samples for which the following data was
129 available: (i) mRNA-seq data from the GEUVADIS project, (ii) SNVs called from whole-
130 genome sequencing data overlaid on the hg38 human reference genome made
131 available by the 1000Genomes project, and (iii) repeat structural variation data made
132 available by the 1000Genomes project. This yielded samples from 358 European and
133 86 Yoruban individuals, all of whom declared themselves to be healthy at the time of
134 sample collection (**Figure 1A**). Using the GEUVADIS data, we obtained gene and TE
135 subfamily expression counts using Tetranscripts²⁷. As a quality control step, we
136 checked whether mapping rates segregated with ancestry groups, which may bias
137 results. However, the samples appeared to cluster by laboratory rather than by ancestry
138 (**Figure S1A**). As additional quality control metrics, we also checked whether the SNV
139 and SV data segregated by ancestry following principal component analysis (PCA).
140 These analyses demonstrated that the top two and the top three principal components
141 from the SNV and SV data, respectively, segregated ancestry groups (**Figure S1B**,
142 **Figure S1C**).

143
144 We then chose to do a three-part integration of the available “omic” data (**Figure**
145 **1B**). Since Tetranscripts quantifies TE expression aggregated at the TE subfamily level
146 and discards TE position information, we chose to carry out a *trans*-eQTL analysis
147 against global expression of each L1 subfamily. We reasoned that there would have to
148 be factors (i.e., miRNAs, proteins, non-coding RNAs) mediating the effects of SNVs on
149 L1 subfamily expression. Thus, to identify candidate genic mediators, we searched for
150 genes with *cis*-eQTLs that overlapped with L1 *trans*-eQTLs. As a final filter, we
151 reasoned that for a subset of regulators, L1 subfamily expression would respond to
152 changes in the expression of those regulators. Consequently, we chose to quantify the
153 association between L1 subfamily expression and candidate gene expression by linear

154 regression. We hypothesized that this three-part integration would result in
155 combinations of significantly correlated SNVs, genes, and L1 subfamilies (**Figure 1B**).

156

157 The *trans*-eQTL analysis against every expressed L1 subfamily led to the
158 identification of 499 *trans*-eQTLs distributed across chromosomes 6, 11, 12, 14, and 15
159 that passed genome-wide significance (**Figure 1C, Supplementary Table S1A**). The
160 *cis*-eQTL analysis led to the identification of 845,260 *cis*-eQTLs that passed genome-
161 wide significance (**Supplementary Figure S2, Supplementary Table S1B**). After
162 integrating the identified *cis*- and *trans*-eQTLs and running linear regression, we
163 identified 1,272 SNV-Gene-L1 trios that fulfilled our three-part integration approach
164 (**Supplementary Table S1C**). Among this pool of trios, we identified 7 unique protein-
165 coding genes including *IL16*, *STARD5*, *HLA-DRB5*, *HLA-DQA2*, *HSD17B12*, *RNF5*, and
166 *FKBPL* (**Figure 1C**). We note that although *EHMT2* did not pass out screening
167 approach, it does overlap *EHMT2-AS1*, which did pass our screening thresholds
168 (**Figure 1C**). We also note that several other unique non-coding genes, often
169 overlapping the protein-coding genes listed, were also identified (**Figure 1C**). For
170 simplicity of interpretation, we focused on protein-coding genes during downstream
171 experimental validation.

172

173 Next, to define first and second tier candidate regulators, we clumped SNVs in
174 linkage disequilibrium (LD) by L1 *trans*-eQTL p-value to identify the most strongly
175 associated genetic variant in each genomic region (**Figure 2A, Supplementary Figure**
176 **S3A**). LD-clumping identified the following index SNVs (*i.e.* the most strongly associated
177 SNVs in a given region): rs11635336 on chromosome 15, rs9271894 on chromosome
178 6, rs1061810 on chromosome 11, rs112581165 on chromosome 12, and rs72691418
179 on chromosome 14 (**Supplementary Table S1D**). Genes linked to these SNVs were
180 considered first tier candidate regulators and included *IL16*, *STARD5*, *HLA-DRB5*, *HLA-*
181 *DQA2*, and *HSD17B12* (**Figure 2B, Supplementary Table S1E**). The remaining genes
182 were linked to clumped, non-index SNVs and were consequently considered second tier
183 candidates and included *RNF5*, *EHMT2-AS1*, and *FKBPL* (**Supplementary Figure**
184 **S3B**). Additionally, for simplicity of interpretation, we considered only non-*HLA* genes

185 during downstream experimental validation, since validation could be complicated by
186 the highly polymorphic nature of *HLA* loci²⁸ and their involvement in multi-protein
187 complexes.

188

189 Finally, to computationally determine whether candidate genes may causally
190 influence L1 subfamily expression, we carried out mediation analysis on all SNV-gene-
191 L1 trios (**Supplementary Figure S4A**). Interestingly, 868 out of the 1,272 (68.2%) trios
192 exhibited significant (FDR < 0.05) mediation effects (**Supplementary Table S1F**).
193 Among the 1st tier candidate regulators, significant, partial, and consistent mediation
194 effects could be attributed to *STARD5*, *IL16*, *HSD17B12*, and *HLA-DRB5*
195 (**Supplementary Figure S4B, Supplementary Table S1F**). To note, while significant
196 mediation could be attributed to the index SNV for *STARD5*, significant mediation could
197 only be attributed to clumped SNVs for *IL16* and *HSD17B12*. Given that *STARD5* and
198 *IL16* share *cis*-eQTL SNVs, this suggests that *STARD5* may be the more potent
199 mediator. Among the 2nd tier candidate regulators, significant, partial, and consistent
200 mediation effects could be attributed to *RNF5*, *EHMT2-AS1*, and *FKBP1*
201 (**Supplementary Figure S4C, Supplementary Table S1F**). These results suggest that
202 candidate genes may mediate the effects between linked SNVs and L1 subfamilies.

203

204

205 *In silico scanning for L1 subfamily candidate regulators in an African population*

206 We next sought to assess the cross-ancestry regulatory properties of candidate
207 genes by repeating our scan using the Yoruban samples as a smaller but independent
208 replication cohort. Here, rather than conduct a genome-wide scan for *cis*- and *trans*-
209 associated factors, we opted for a targeted approach focusing only on gene *cis*-eQTLs
210 and L1 subfamily *trans*-eQTLs that were significant in the analysis with European
211 samples (**Supplementary Figure S5A**). The targeted *trans*-eQTL analysis led to the
212 identification of 227 significant (FDR < 0.05) *trans*-eQTLs distributed across
213 chromosomes 6 and 11 (**Supplementary Table S2A**). The targeted *cis*-eQTL analysis
214 led to the identification of 1,248 significant (FDR < 0.05) *cis*-eQTLs (**Supplementary**
215 **Table S2B**). After integrating the identified *cis*- and *trans*-eQTLs and running linear

216 regression, we identified 393 SNV-Gene-L1 trios that fulfilled our three-part integration
217 approach (**Supplementary Table S2C**). Among this pool of trios, we identified 2 unique
218 protein-coding genes—*HSD17B12* and *HLA-DRB6*—as well as several unique non-
219 coding genes (**Supplementary Table S2C**). Again, we clumped SNVs in linkage
220 disequilibrium (LD) by L1 *trans*-eQTL p-value. LD-clumping identified the following index
221 SNVs: rs2176598 on chromosome 11 and rs9271379 on chromosome 6
222 (**Supplementary Table S2D**). Genes linked to these SNVs were considered first tier
223 candidate regulators and included both *HSD17B12* and *HLA-DRB6* (**Supplementary**
224 **Figure S5B, Supplementary Table S2E**). Finally, we carried out mediation analysis on
225 all SNV-gene-L1 trios; however, no significant (FDR < 0.05) mediation was observed
226 (**Supplementary Table S2F**). These results implicate *HSD17B12* and the *HLA* loci as
227 candidate, cross-ancestry L1 expression regulators.

228

229 To assess why some candidate genes did not replicate in the Yoruba cohort, we
230 manually inspected *cis*- and *trans*-eQTL results for trios with those genes
231 (**Supplementary Figure S6A**). Interestingly, we identified rs9270493 and rs9272222 as
232 significant (FDR < 0.05) *trans*-eQTLs for L1MEb expression. However, those SNVs
233 were not significant *cis*-eQTLs for *RNF5* and *FKBP1* expression, respectively. For trios
234 involving *STARD5*, *IL16*, and *EHMT2-AS1*, neither the *cis*-eQTL nor the *trans*-eQTL
235 were significant. We note that for most of these comparisons, although the two
236 genotypes with the largest sample sizes were sufficient to establish a trending change
237 in *cis* or *trans* expression, this trend was often broken by the third genotype with
238 spurious sample sizes. This suggests that replication in the Yoruba cohort may be
239 limited by the small cohort sample size in the GEUVADIS project.

240

241

242 *TE families and known TE-associated pathways are differentially regulated across L1*
243 *trans-eQTL variants*

244 Though our eQTL analysis identified genetic variants associated with the
245 expression of specific, evolutionarily older L1 subfamilies, we reasoned that there may
246 be more global but subtle differences in TE expression profiles among genotype groups,

247 given that TE expression is highly correlated²¹. Thus, for each gene-associated index
248 SNV identified in the European eQTL analysis, we carried out differential expression
249 analysis for all expressed genes and TEs (**Supplementary Table S3A-S3C; Figure**
250 **3A**). At the individual gene level, we detected few significant (FDR < 0.05) changes: 4
251 genes/TEs varied with rs11635336 genotype (*IL16/STARD5*), 4 genes/TEs varied with
252 rs9271894 genotype (*HLA*), and 5 gene/TEs varied with rs1061810 genotype
253 (*HSD17B12*) (**Supplementary Table S3A-S3C**). Importantly, however, these
254 genes/TEs overlapped the genes/TEs identified in the *cis*- and *trans*-eQTL analyses,
255 providing an algorithmically independent link among candidate SNV-gene-TE trios.

256 In contrast to gene-level analyses, Gene Set Enrichment Analysis (GSEA)
257 provides increased sensitivity to subtle but consistent/widespread transcriptomic
258 changes at the level of gene sets (e.g. TE families, biological pathways, etc.). Thus, we
259 leveraged our differential expression analysis in combination with GSEA to identify
260 repeat family and biological pathway gene sets impacted by SNV genotype in the
261 GEUVADIS dataset (**Supplementary Table S3D-S3O; Figure 3A**). Interestingly,
262 changes in the genotype of rs11635336 (*IL16/STARD5*), rs9271894 (*HLA*), and
263 rs1061810 (*HSD17B12*) were associated with an upregulation, upregulation, and
264 downregulation, respectively, of multiple TE family gene sets (**Figure 3B,**
265 **Supplementary Table S3P**). Differentially regulated TE family gene sets included DNA
266 transposons, such as the hAT-Charlie family, and long terminal repeat (LTR)
267 transposons, such as the endogenous retrovirus-1 (ERV1) family (**Figure 3B,**
268 **Supplementary Table S3P**). Noteworthy, the L1 family gene set was the only TE gene
269 set whose expression level was significantly altered across all three SNV analyses
270 (**Figure 3B, Supplementary Table S3P**). Consistent with their relative significance in
271 the L1 *trans*-eQTL analysis, the L1 family gene set was most strongly upregulated by
272 alternating the *IL16/STARD5* SNV (NES = 3.74, FDR = 6.43E-41), intermediately
273 upregulated by alternating the *HLA* SNV (NES = 1.90, FDR = 7.19E-5), and least
274 strongly changed by alternating the *HSD17B12* SNV (NES = -1.57, FDR = 2.11E-2)
275 (**Figure 3C**). We briefly note here that rs9270493, a clumped SNV linked to *RNF5*, was
276 also linked to upregulation of the L1 family gene set (**Supplementary Table S3Q-S3R**).

277 These results suggest that TE subfamily *trans*-eQTLs are associated with subtle but
278 global differences in TE expression beyond a lone TE subfamily.

279

280 Next, we asked if other biological pathways were regulated concomitantly with
281 TE gene sets in response to gene-linked index SNVs, reasoning that such pathways
282 would act either upstream (as regulatory pathways) or downstream (as response
283 pathways) of TE alterations. GSEA with the MSigDB Hallmark pathway gene sets^{29,30}
284 identified 5 gene sets fitting this criterion, including “oxidative phosphorylation”,
285 “mTORC1 signaling”, “fatty acid metabolism”, “adipogenesis”, and “cholesterol
286 homeostasis” (**Figure 3D, Supplementary Table S3S**). Interestingly, several of these
287 pathways or genes in these pathways have been implicated in TE regulation before.
288 Rapamycin, which acts through mTORC1, has been shown to alter the expression of L1
289 and other repeats^{31,32}. Estrogens, which are involved in cholesterol and lipid
290 metabolism, have been found to drive changes in repeat expression, and the receptors
291 for both estrogens and androgens are believed to bind repeat DNA^{32,33}.
292 Pharmacological inhibition of the mitochondrial respiratory chain and pharmacological
293 reduction of endogenous cholesterol synthesis have also been shown to induce
294 changes in L1 protein levels or repeat expression more broadly^{34,35}. GSEA with the GO
295 Biological Process gene sets (**Figure 3E, Supplementary Table S3T**) and the
296 Reactome gene sets (**Figure 3F, Supplementary Table S3U**) also identified several
297 metabolism-related pathways including “ATP metabolic process”, “Generation of
298 precursor metabolites and energy”, and “metabolism of amino acids and derivatives”.
299 These results add to the catalogue of pathways associated with differences in L1
300 expression.

301

302 In our eQTL analysis, we also identified two orphan index SNVs, rs112581165
303 and rs72691418, to which we could not attribute a protein-coding gene mediator. To
304 determine whether these SNVs also regulate any transposon families or biological
305 pathways, we repeated the differential expression analysis (with all expressed genes
306 and TEs) (**Supplementary Table S4A-S4B**) and the GSEA (**Supplementary Table**
307 **S4C-S4J**) with these SNVs (**Supplementary Figure S7A**). At the individual gene level,

308 we detected 3193 genes/TEs that varied significantly (FDR < 0.05) with rs112581165
309 genotype and 1229 genes/TEs that varied significantly with rs72691418 genotype
310 (**Supplementary Table S4A-S4B**). Similar to above, we next carried out GSEA to
311 identify changes in functionally relevant gene sets. Like the gene-linked index SNVs,
312 changes in the genotype of rs112581165 and rs72691418 were both associated with a
313 downregulation and upregulation, respectively, of 10 TE families (**Supplementary**
314 **Figure S7B, Supplementary Table S4K**). Noteworthy, the L1 family gene set was
315 among the most strongly dysregulated TE family gene sets for both rs112581165 (NES
316 = -4.32, FDR = 5.18E-89) and rs72691418 (NES = 4.01, FDR = 5.38E-79)
317 (**Supplementary Figure S7C**). These results suggest that TE subfamily *trans*-eQTLs
318 are associated with subtle differences in TE expression beyond the lone TE subfamily,
319 even in the absence of a protein-coding gene *cis*-eQTL.

320

321 Like before, we asked if other biological pathways were regulated concomitantly
322 with TE gene sets in response to orphan index SNVs. The top 10 Hallmark pathway
323 gene sets identified by GSEA included gene sets that were previously identified
324 (“oxidative phosphorylation”, “fatty acid metabolism”, and “mTORC1 signaling”), as well
325 as several new pathways (**Supplementary Figure S7D, Supplementary Table S4L**).
326 Among the new pathways, “DNA repair”²⁰ and the “P53 pathway”^{36,37} have also been
327 linked to L1 control, and proteins in the “Myc targets v1” gene set interact with L1
328 ORF1p³⁸. GSEA with the GO Biological Process gene sets (**Supplementary Figure**
329 **S7E, Supplementary Table S4M**) and the Reactome gene sets (**Supplementary**
330 **Figure S7F, Supplementary Table S4N**) identified several metabolism-related
331 pathways and several translation-related pathways, such as “cytoplasmic translation”,
332 “eukaryotic translation initiation”, and “eukaryotic translation elongation”. Importantly,
333 proteins involved in various aspects of proteostasis have been shown to be enriched
334 among L1 ORF1p-interacting proteins³⁸. Again, these results add to the catalogue of
335 pathways associated with differences in TE expression, even in the absence of a
336 candidate *cis* mediator.

337

338

339 *Modulation of top candidate gene activity in a lymphoblastoid cell line induces small but*
340 *widespread TE expression changes*

341 We decided to validate the L1 regulatory properties of top candidate genes
342 associated with L1 *trans*-eQTLs. For experimental purposes, we selected the GM12878
343 lymphoblastoid cell line, because (i) it is of the same cell type as the transcriptomic data
344 used here for our eQTL analysis, and (ii) its epigenomic landscape and culture
345 conditions have been well well-characterized as part of the ENCODE project^{39,40}. For
346 validation purposes, we selected *IL16*, *STARD5*, *HSD17B12*, and *RNF5* out of the 7
347 protein-coding gene candidates. We chose these genes for validation because the first
348 3 are associated with top *trans*-eQTL SNVs and the fourth one had very strong
349 predicted mediation effects. To note, although GM12878 was part of the 1000Genomes
350 Project, it was not included in the GEUVADIS dataset. However, based on its genotype,
351 we can predict the relative expression of candidate regulators (**Supplementary Figure**
352 **S8A**), which suggest that GM12878 may be most sensitive to modulations in *IL16* and
353 *STARD5* expression, given their relatively low endogenous expression. Interestingly,
354 examination of the ENCODE epigenomic data in GM12878 cells³⁹ demonstrated that
355 the region near the *IL16/STARD5*-linked index SNV (rs11635336) was marked with
356 H3K4Me1 and H3K27Ac, regulatory signatures of enhancers (**Supplementary Figure**
357 **S8C**). Similarly, the region near the *HLA*-linked index SNV (rs9271894) was marked
358 with H3K4Me1, marked with H3K27Ac, and accessible by DNase, suggesting regulatory
359 properties of the region as an active enhancer (**Supplementary Figure S8C**). These
360 results further highlight the regulatory potential of the *IL16*-, *STARD5*-, and *HLA*-linked
361 SNVs.

362

363 First, we decided to test the transcriptomic impact of overexpressing our top
364 candidates in GM12878 LCLs. Cells were electroporated with overexpression plasmids
365 (or corresponding empty vector), and RNA was isolated after 48h (**Figure 4A**,
366 **Supplementary Figure S9A**). Differential expression analysis comparing control and
367 overexpression samples confirmed the overexpression of candidate genes
368 (**Supplementary Figure S9B**, **Supplementary Table S5A-S5D**). Intriguingly, we
369 observed that *IL16* was significantly upregulated following *STARD5* overexpression

370 **(Supplementary Figure S9C, Supplementary Table S5B)**, although the inverse was
371 not observed **(Supplementary Figure S9C, Supplementary Table S5A)**, suggesting
372 that *IL16* may act downstream of *STARD5*. We note here that, consistent with the use
373 of a high expression vector, the *IL16* upregulation elicited by *STARD5* overexpression
374 (\log_2 fold change = 0.45) was weaker than the upregulation from the *IL16*
375 overexpression (\log_2 fold change = 1.89) **(Supplementary Table S5A-S5B)**.

376

377 To further assess the biological relevance of each overexpression, we carried out
378 GSEA using the GO Biological Process, Reactome pathway, and Hallmark pathway
379 gene sets **(Supplementary Table S5E-S5P)**. Importantly, GSEA using GO Biological
380 Process and Reactome pathway gene sets highlighted differences that were consistent
381 with the known biology of our candidate genes. Firstly, *IL16* is involved in regulating T-
382 cell activation, B-cell differentiation, and functions as a chemoattractant⁴¹⁻⁴⁶. Moreover,
383 it modulates macrophage polarization by regulating *IL-10* expression⁴⁷. *IL16*
384 overexpressing cells showed upregulation for “phagocytosis recognition” and “positive
385 chemotaxis”, downregulation for “negative regulation of cell differentiation”, and
386 downregulation for “Interleukin 10 signaling” **(Figure 4B-4C)**. Secondly, *STARD5*
387 encodes a cholesterol transporter and is upregulated in response to endoplasmic
388 reticulum (ER) stress⁴⁸⁻⁵⁰. *STARD5* overexpressing cells showed downregulation of
389 various cholesterol-related gene sets such as “sterol biosynthetic process”, “sterol
390 metabolic process”, and “regulation of cholesterol biosynthesis by SREBP (SREBF)”
391 **(Figure 4D-4E)**. Thirdly, *HSD17B12* encodes a steroid dehydrogenase involved in
392 converting estrone into estradiol and is essential for proper lipid homeostasis⁵¹⁻⁵³.
393 *HSD17B12* overexpressing cells showed downregulation of cholesterol-related gene
394 sets, including “sterol biosynthetic process” and “regulation of cholesterol biosynthesis
395 by SREBF (SREBP)” **(Supplementary Figure S9D-S9E)**. Finally, *RNF5* encodes an
396 ER and mitochondrial-bound E3 ubiquitin-protein ligase that ubiquitin-tags proteins for
397 degradation⁵⁴⁻⁵⁷. *RNF5* overexpressing cells demonstrated alterations in gene sets
398 involved in proteostasis and ER biology, including upregulation of “ERAD pathway”,
399 “response to endoplasmic reticulum stress”, and “intra-Golgi and retrograde Golgi-to-ER
400 traffic” **(Supplementary Figure S9F-S9G)**. These results suggest that our approach

401 leads to biological changes consistent with the known biological impact of the genes
402 being overexpressed.

403

404 Next, we sought to determine whether modulation of candidate genes had any
405 impact on TE expression in general, and L1 in particular. Although there were no
406 significant changes for individual TE subfamilies following *IL16* and *STARD5*
407 overexpression (**Supplementary Table S5A-S5B**), we identified subtle but widespread
408 upregulation of various TE families across both conditions by GSEA (**Figure 4F**,
409 **Supplementary Table S5Q-S5R**). Interestingly, 7 families, including L1, ERV1, ERVL-
410 MaLR, Alu, ERVL, TcMar-Tigger, and hAT-Charlie families, were commonly
411 upregulated under both conditions (**Figure 4F**). In contrast, cells overexpressing
412 *HSD17B12* or *RNF5* did not drive widespread changes in L1 family expression, as
413 assessed by GSEA (**Supplementary Table S5S-S5T**). Noteworthy, the L1 family gene
414 set was more strongly upregulated following *STARD5* overexpression (NES = 2.25,
415 FDR = 6.14E-7) compared to *IL16* overexpression (NES = 2.24, FDR = 2.40E-5)
416 (**Figure 4G, Supplementary Table S5Q-S5R**). Since *IL16* is upregulated in response to
417 *STARD5* overexpression, this suggests that *STARD5* may synergize with *IL16* for the
418 regulation of L1 transcription.

419

420 Then, we decided to further characterize the impact of IL16 activity on TEs, since
421 (i) its overexpression led to a global upregulation of TE transcription, and (ii) it was itself
422 upregulated in response to *STARD5* overexpression, which also led to increased TE
423 expression. Thus, since IL16 is a soluble cytokine, we independently assessed its
424 regulatory properties by exposing GM12878 cells to recombinant human IL16 peptide
425 [rhIL16] for 24 hours (**Figure 5A, Supplementary Figure S10A**). Differential gene
426 expression analysis (**Supplementary Table S6A**) and comparison with the *IL16*
427 overexpression results demonstrated that differentially expressed genes were weakly
428 but significantly correlated (**Supplementary Figure S10B**). Additionally, we carried out
429 GSEA using the GO Biological Process, Reactome pathway, and Hallmark pathway
430 gene sets (**Supplementary Table S6B-S6E**) and compared those results with the
431 GSEA from the *IL16* overexpression (**Supplementary Table S6F-S6H**). Consistent with

432 the known biology of *IL16*, GSEA highlighted a downregulation of many immune cell-
433 related gene sets, including “leukocyte differentiation”, “mononuclear cell differentiation”,
434 and “Interleukin-10 signaling” (**Figure 5B-5C, Supplementary Table S6F-S6H**). Like
435 the overexpression results, exposure of GM12878 to rhIL16 for 24 hours led to an
436 upregulation of an L1 family gene set by GSEA, although the effect was less
437 pronounced than with the overexpression (**Figure 5D**). Even though treatment of
438 GM12878 with rhIL16 for 48 hours exhibited known features of IL16 biology
439 (**Supplementary Figure S10B-S10D, Supplementary Table S6J-S6Q**), the L1
440 upregulation was no longer detectable, though other TEs remained upregulated
441 (**Supplementary Figure S10E, Supplementary Table S6Q**). These results further
442 support the notion that *IL16* acts as a modulator of L1 expression.

443
444 Finally, we sought to define the biological pathways regulated concomitantly with
445 the L1 family gene set under all experimental conditions where it was upregulated (i.e.,
446 *IL16* overexpression, *STARD5* overexpression, and 24 hours of rhIL16 exposure)
447 (**Figure 6A, Figure 6B, Supplementary Table S7A**). Again, we reasoned that such
448 pathways would act either upstream (as regulatory pathways) or downstream (as
449 response pathways) of TE alterations. GSEA with the Hallmark pathway gene sets
450 identified 7 gene sets fitting this criterion, including “TNF α signaling via NF-KB”, “IL2
451 STAT5 signaling”, “inflammatory response”, “mTORC1 signaling”, “estrogen response
452 early”, “apoptosis”, and “UV response up” (**Figure 6C, Supplementary Table S7B**).
453 GSEA with the GO Biological Process gene sets (**Figure 6D, Supplementary Table**
454 **S7C**) and the Reactome pathway gene sets (**Figure 6E, Supplementary Table S7D**)
455 also identified MAPK signaling, virus-related pathways like “HCMV early events”,
456 pathways involved in cell differentiation, and pathways involved in cholesterol and
457 steroid metabolism like “signaling by nuclear receptors”. These results further cement
458 the catalogue of pathways associated with differences in TE expression.

459

460

461 *L1 trans-eQTLs are co-associated with aging traits in GWAS databases.*

462 Although TE de-repression has been observed broadly with aging and age-
463 related disease^{5,58}, whether this de-repression acts as a causal driver, or a downstream
464 consequence, of aging phenotypes remains unknown. We reasoned that if increased
465 TE expression at least partially drives aging phenotypes, L1 *trans*-eQTLs should be
466 enriched for associations to aging traits in genome-wide association studies [GWAS] or
467 phenome-wide association studies [PheWAS].

468
469 To test our hypothesis, we queried the Open Targets Genetics platform with our
470 499 *trans*-eQTL SNVs, mapped traits to standardized MeSH IDs, and then manually
471 curated MeSH IDs related to aging-related traits (**Figure 7A**). Consistent with our
472 hypothesis, a large proportion of L1 *trans*-eQTL SNVs (222/499 or 44.5%) were either
473 (i) associated with an aging MeSH trait by PheWAS or (ii) LD-linked to a lead variant
474 associated with an aging MeSH trait (**Figure 7B**). Moreover, among the 222 SNVs with
475 significant aging-trait associations, we observed frequent mapping to more than a single
476 age-related trait by PheWAS, with many SNVs associated with 10-25 traits (**Figure 7C**,
477 **Supplementary Table S8A**). Additionally, many of the 222 SNVs mapped to 1-5 aging
478 traits through a proxy lead variant (**Figure 7D, Supplementary Table S8A**). Among the
479 most frequently associated or linked traits, we identified type 2 diabetes mellitus,
480 hyperparathyroidism, thyroid diseases, coronary artery disease, hypothyroidism, and
481 psoriasis, among many others (**Figure 7E, Supplementary Table S8B**).

482
483 As a parallel approach, we queried the Open Targets Genetics platform with our
484 L1 *trans*-eQTL SNVs, as well as 500 combinations of random SNVs sampled from all
485 SNVs used in the eQTL analyses. We then leveraged broader phenotype categories
486 annotated by the platform, including 14 disease categories that we considered aging-
487 related, to determine whether L1 eQTL associations were enriched for any disease
488 categories (**Supplementary Figure S11A**). L1 eQTL associations were significantly
489 enriched (FDR < 0.05 and ES > 1) for 13 out of 14 disease categories, including cell
490 proliferation disorders, immune system diseases, and musculoskeletal diseases
491 (**Supplementary Figure S11B-N**). The cardiovascular diseases category was the only
492 disease category for which we did not observe a significant enrichment

493 **(Supplementary Figure S110)**. The enrichment for cell proliferation disorders is
494 consistent with the associations of L1 activity with cellular senescence^{12,15} and cancer
495^{59,60}. The enrichment for immune system diseases is consistent with the role of L1 as a
496 stimulator of the interferon pathway, inflammation, and senescence¹⁵, as well as the
497 more general notion that transposons can mimic viruses and stimulate immune
498 responses from their hosts⁶¹. The enrichment for musculoskeletal diseases is
499 consistent with an increase in L1 expression and copy number with age in muscle tissue
500 from aging mice¹¹. These results reinforce the notion that L1 activity is strongly and
501 non-randomly associated with an assortment of age-related diseases.

502

503 Intriguingly, a large fraction of co-associated SNVs were on chromosome 6 near
504 the HLA locus, which has previously been shown to be a hotspot of age-related disease
505 traits⁶². Despite its association to our strongest L1 trans-eQTL SNV, little is known
506 about the regulation and impact of IL16 during aging. One study, however, found that
507 *IL16* expression increases with age in ovarian tissue, and the frequency of *IL16*
508 expressing cells is significantly higher in ovarian tissue from women at early and late
509 menopause, compared to premenopausal women⁶³. Given these findings, and since L1
510 expression levels and copy number have been found to increase with age⁵, we asked
511 whether circulating IL16 levels may also change with age, using C57BL/6JNia mice as a
512 model **(Figure 7F, Supplementary Table S8C)**. Consistent with the notion that
513 increased IL16 levels may, at least partially, drive age-related TE de-repression, we
514 observed a significant increase in circulating IL16 levels in female mice with age, and a
515 trending increase with age in male mice (although the levels showed more animal-to-
516 animal variability). By meta-analysis, circulating IL16 levels changed significantly with
517 age across sexes **(Figure 7F)**. These results further support the hypothesis that *IL16* is
518 involved in L1 biology and may modulate L1 age-related changes. In sum, our results
519 provide one of the first pieces of evidence of a causal link between L1 expression levels
520 and age-related decline.

521

522 **Discussion**

523 *A new approach to identify regulators of TE expression*

524 In this work, we developed a pipeline to computationally identify candidate L1
525 transcriptional regulators by eQTL analysis. We provide experimental evidence for the
526 involvement of top candidates in regulating L1 expression, demonstrating as a proof-of-
527 principle that this approach can be broadly used on other large “omic”-characterized
528 cohorts with human (i.e. GTEx^{64,65} or HipSci⁶⁶) or mouse (i.e. DO mice⁶⁷) subjects to
529 identify other regulators of L1 activity. These datasets, combined with our approach,
530 could be utilized to rigorously characterize conserved or group-specific TE regulatory
531 mechanisms on multiple layers, such as across TE families (like Alu or ERVs), across
532 cell or tissue types, across ancestry groups, and across species. This approach, which
533 leverages existing datasets to perform *in silico* screening, could be a powerful method
534 to expand our knowledge of TE regulation in non-diseased cells and tissues.

535 Though our initial scan identified genetic variants associated with expression
536 differences in specific L1 subfamilies, secondary analyses by GSEA suggest that
537 genetic variants are associated with subtle but global differences in the expression of
538 many TE families. Our pipeline identified candidate genes, including *HSD17B12* and
539 *HLA* genes, that likely play a conserved role in L1 regulation across human populations
540 of different ancestries. Though some top candidates from the European cohort scan,
541 such as *IL16*, *STARD5*, and *RNF5*, were not significant in the African cohort analysis, it
542 is likely that some of these genes would appear in cross-ancestry scans with larger
543 samples sizes. We detected subtle but global differences in L1 family expression
544 following *IL16* overexpression, *STARD5* overexpression, and rhIL16 treatment for 24
545 hours, further suggesting that our top candidates have regulatory potential.

546

547 *New candidate L1 regulators are involved in viral response*

548 As another, theoretical line of evidence for the potential involvement of our top
549 candidate genes in L1 regulation, we highlight known interactions between tested
550 candidate genes and viral infections, which may be relevant under conditions where
551 transposons are recognized as viral mimics⁶¹. Indeed, *IL16* has been extensively
552 studied for its ability to inhibit human immunodeficiency virus (HIV) replication, partly by

553 suppressing mRNA expression⁶⁸⁻⁷⁰. Additionally, but in contrast to its HIV-suppressive
554 properties, *IL16* can enhance the replication of influenza A virus (IAV) and facilitate its
555 infection of hosts, potentially through its repression of type I interferon beta and
556 interferon-stimulated genes⁷¹. *IL16* can also contribute to the establishment of lifelong
557 gamma herpesvirus infection⁷². *STARD5* is another candidate implicated in the
558 influenza virus replication cycle⁷³. *HSD17B12* promotes the replication of hepatitis C
559 virus via the very-long-chain fatty acid (VLCFA) synthesis pathway and the production
560 of lipid droplets important for virus assembly^{74,75}. Additionally, *HSD17B12* has been
561 found interacting with the coronavirus disease 2019 (COVID-19) protein nonstructural
562 protein 13 (NSP13), which is thought to antagonize interferon signaling⁷⁶. Finally, *RNF5*
563 has been implicated in both promoting and antagonizing severe acute respiratory
564 syndrome coronavirus 2 (SARS-CoV-2) by either stabilizing the interactions of
565 membrane protein (M)⁷⁷ or inducing degradation of structural protein envelope (E)⁷⁸,
566 respectively. Fundamentally, *RNF5* regulates virus-triggered interferon signaling by
567 targeting the stimulator of interferon genes (STING) or mitochondrial antiviral signaling
568 protein (MAVS) for ubiquitin-mediated protein degradation^{56,57}. These studies reinforce
569 the roles of tested candidate regulators in virus-associated processes, including
570 interferon-mediated signaling.

571

572

573 *Future considerations for the use of trans-eQTL analysis in identification of L1*
574 *regulators*

575 While we believe our approach can readily be applied to other datasets, we
576 would like to note potential further considerations with the approach we implemented,
577 some of which were simply beyond the scope of this paper. Firstly, though it is common
578 to use probabilistic estimation of expression residuals (PEER)⁷⁹ to enhance detection of
579 *cis*-eQTLs, PEER was not implemented in our analysis as a precautionary measure, in
580 order to avoid potentially blurring global TE signals, which likely led to a more
581 conservative list of candidate *cis* gene mediators. Second, given the technical
582 complexity in generating the vast amount of mRNA-seq data used for the eQTL
583 analysis, it is possible that technical covariates introduced non-linear effects that would

584 not be easily removed by approaches like PEER or SVA⁸⁰. For that reason, we opted to
585 supplement our computational predictions with experimental data. Third, the L1 *trans*-
586 eQTLs identified were specific to older L1 subfamilies (L1P and L1M) and were not
587 shared across subfamilies. One factor that may partially explain this is the heightened
588 difficulty of quantifying the expression of evolutionarily younger L1 subfamilies using
589 short-read sequencing⁸¹.

590 More generally, significant single gene differences are often difficult to reproduce
591 across studies, and it is for this reason that methods like GSEA were developed, to
592 robustly identify broader changes in sets of genes²⁹. Consistently, GSEA suggests that
593 many TE families, beyond the single L1 subfamilies identified in the eQTL analysis, are
594 differentially regulated among samples with different genotypes for *trans*-eQTL SNVs
595 and among samples where *IL16/IL16* and *STARD5* were manipulated. We note that
596 although *HLA* and *HSD17B12* loci were significant in both the European and African
597 cohorts, we were not able to independently identify all of the same candidate regulators.
598 This is likely due to a combination of small sample size for the African cohort and the
599 existence of population-specific L1 regulation. Future studies with larger sample sizes
600 may be useful for expanding the catalogue of loci that are biologically meaningful for L1
601 expression across more than one population. Importantly, our computational scan is
602 limited to loci exhibiting genomic variation among tested individuals. This will vary with
603 factors like the ancestry groups of the populations being studied. Moreover, variants
604 that confer extreme fitness defects may not exist at a sufficiently high level in a
605 population to allow for an assessment of their involvement as eQTLs.

606 Finally, although we focused on protein-coding candidate regulators, it is possible
607 that the non-coding genes identified in our scan may also causally drive differences in
608 L1 expression. Though not explored here, other regulatory factors like small RNAs may
609 also act as partial mediators. Since the GEUVADIS Consortium generated small RNA
610 data in parallel to the mRNA data used in this study²⁶, a future application of our
611 pipeline could be to scan for *cis* small RNA mediators in the same biological samples.
612 These unexplored factors may explain the associations between orphan SNV
613 genotypes and TE family gene set changes.

614

615 *L1 trans-eQTLs are enriched for genetic variants linked to aging and age-related*
616 *disease*

617 Consistent with the notion that L1 is associated with aging and aging phenotypes
618 ^{5,58}, we observed that L1 *trans*-eQTL SNVs were associated with aging phenotypes in
619 GWAS/PheWAS databases. This is very surprising, but interesting, given that all
620 1000Genomes Project participants declared themselves to be healthy at the time of
621 sample collection. Assuming this to be true, our results suggest that L1 expression
622 differences exist in natural, healthy human populations, and these expression
623 differences precede onset of aging diseases. Though it is often unclear whether L1 mis-
624 regulation is a consequence or driver of aging phenotypes, our results suggest that L1
625 levels may drive aging phenotypes. As we continue to expand the catalogue of L1
626 regulators, especially in healthy cells and tissues, the L1 regulatory processes that are
627 disrupted over the course of aging will become increasingly clear. To that end, this work
628 may serve as a guide for conducting more comprehensive scans for candidate TE
629 regulators.

630

631 In summary, we developed an eQTL-based pipeline that leverages genomic and
632 transcriptomic data to scan the human genome for novel candidate regulators of L1
633 subfamily expression. Though the initial scan identified genetic variants associated with
634 expression differences in specific L1 subfamilies, secondary analyses by GSEA suggest
635 that genetic variants are associated with subtle but global differences in the expression
636 of many TE families. Our pipeline identified candidate genes, including *HSD17B12* and
637 *HLA* genes, that likely play a conserved role in L1 regulation across human populations
638 of different ancestries. Though some top candidates from the European cohort scan,
639 such as *IL16*, *STARD5*, and *RNF5*, were not significant in the African cohort analysis, it
640 is likely that some of these genes would appear in cross-ancestry scans with larger
641 sample sizes. We detected subtle but global differences in L1 family expression
642 following *IL16* overexpression, *STARD5* overexpression, and rhIL16 treatment for 24
643 hours, further suggesting that some candidate genes have regulatory potential. We
644 generate a list of pathways, such as mTORC1 signaling and cholesterol metabolism,
645 that may act upstream of L1 expression. Finally, the co-association of some genetic

646 variants with both L1 expression differences and various age-related diseases suggests
647 that L1 differences may precede and contribute to the onset of disease. Our results
648 expand the potential mechanisms by which L1 expression is regulated and by which L1
649 may influence aging-related phenotypes.
650

651 **Material and Methods**

652 **Publicly available data acquisition**

653 The eQTL analysis was carried out on 358 European (EUR) individuals and 86
654 Yoruban (YRI) individuals for which paired single nucleotide variant, structural variant,
655 and transcriptomic data were available from Phase 3 of the 1000 Genomes Project ^{22,23}
656 and from the GEUVADIS consortium ²⁶. Specifically, Phase 3 autosomal SNVs called
657 on the GRCh38 reference genome were obtained from The International Genome
658 Sample Resource (IGSR) FTP site (
659 [http://ftp.1000genomes.ebi.ac.uk/vol1/ftp/data_collections/1000_genomes_project/relea](http://ftp.1000genomes.ebi.ac.uk/vol1/ftp/data_collections/1000_genomes_project/release/20190312_biallelic_SNV_and_INDEL/)
660 [se/20190312_biallelic_SNV_and_INDEL/](http://ftp.1000genomes.ebi.ac.uk/vol1/ftp/data_collections/1000_genomes_project/release/20190312_biallelic_SNV_and_INDEL/)). Structural variants were also obtained from
661 the IGSR FTP site
662 (http://ftp.1000genomes.ebi.ac.uk/vol1/ftp/phase3/integrated_sv_map/). mRNA-
663 sequencing fastq files generated by the GEUVADIS consortium were obtained from
664 ArrayExpress under accession E-GEUV-1.

665

666 **Aggregating and pre-processing genotype data for eQTL analyses**

667 To prepare SNVs for association analyses, all SNVs were first annotated with
668 rsIDs from dbSNP build 155 using BCFtools v1.10.2 ⁸². VCFtools v0.1.17 ⁸³ was then
669 used to remove indels and keep variants with the following properties in each of the two
670 populations: possessed a minimum and maximum of two alleles, possessed a minor
671 allele frequency (MAF) of at least 1%, passed Hardy-Weinberg equilibrium thresholding
672 at $p < 1e-6$, with no missing samples, and located on an autosome. We note here that
673 sex chromosomes were not included in the analysis since (i) Y chromosome SNVs were
674 not available and (ii) analyses with X chromosome SNVs require unique algorithms and
675 cannot simply be incorporated into traditional association pipelines ^{84,85}. VCF files
676 containing these filtered SNVs were then converted to PLINK BED format using PLINK
677 v1.90b6.17 ⁸⁶, keeping the allele order. PLINK BED files were subsequently used to
678 generate preliminary 0/1/2 genotype matrices using the '--recodeA' flag in PLINK. These
679 preliminary matrices were manipulated in terminal, using the gcut v9.0 function to
680 remove unnecessary columns and datamash v1.7 to transpose the data, to generate
681 the final 0/1/2 matrices used for the eQTL analyses. Finally, PLINK was used to prune

682 the list of filtered SNVs, using the “--indep-pairwise 50 10 0.1” flag, and to generate
683 principal components (PCs) from the pruned genotypes.

684

685 To control for inter-individual differences in genomic transposon copy number
686 load, we applied 1 of 2 approaches, depending on the analysis. For approach 1, the net
687 number of L1 and Alu insertions was quantified across the 444 samples. We chose to
688 aggregate the L1 and Alu copy numbers, since Alu relies on L1 machinery for
689 mobilization⁸⁷, and so the aggregate number may provide a finer view of L1-associated
690 copy number load. Briefly, VCFTools was used to extract autosomal structural variants
691 from the 1000Genomes structural variant calls. L1 and Alu insertions and deletions
692 were then extracted with BCFtools by keeping entries with the following expressions:
693 ‘SVTYPE=“LINE1”’, ‘SVTYPE=“ALU”’, ‘SVTYPE=“DEL_LINE1”’, and
694 ‘SVTYPE=“DEL_ALU”’. The resulting VCF files were then transformed to 0/1/2 matrices
695 in the same manner as the SNVs. A net copy number score was obtained for each
696 sample by adding the values for the L1 and Alu insertions and subtracting the values for
697 the L1 and Alu deletions. For approach 2, the complete structural variant matrix was
698 filtered with VCFtools using the same parameters as with the SNV matrices. The filtered
699 structural variant matrix was then pruned with PLINK, and these pruned structural
700 variant genotypes were used to generate principal components, in the same fashion as
701 with the SNV matrix. The net copy number score or the structural variant principal
702 components, depending on the analysis, were included as covariates.

703

704

705 **mRNA-seq read trimming, mapping, and quantification**

706 Fastq files were first trimmed using fastp v0.20.1⁸⁸ with the following parameters:
707 detect_adapter_for_pe, disable_quality_filtering, trim_front1 17, trim_front2 17,
708 cut_front, cut_front_window_size 1, cut_front_mean_quality 20, cut_tail,
709 cut_tail_window_size 1, cut_tail_mean_quality 20, cut_right, cut_right_window_size 5,
710 cut_right_mean_quality 20, and length_required 36. Read quality was then inspected
711 using fastqc v0.11.9.

712

713 Next, the GRCh38 primary human genome assembly and comprehensive gene
714 annotation were obtained from GENCODE release 33⁸⁹. Since LCLs are generated by
715 infecting B-cells with Epstein-Barr virus, the EBV genome (GenBank ID V01555.2) was
716 included as an additional contig in the human reference genome. The trimmed reads
717 were aligned to this modified reference genome using STAR v2.7.3a⁹⁰ with the
718 following parameters: `outFilterMultimapNmax 100`, `winAnchorMultimapNmax 100`, and
719 `outFilterMismatchNoverLmax 0.04`. Finally, the TEcount function in the Tetranscripts
720 v2.1.4²⁷ package was employed to obtain gene and TE counts, using the GENCODE
721 annotations to define gene boundaries and a repeat GTF file provided on the Hammell
722 lab website (downloaded on February 19 2020 from
723 [https://labshare.cshl.edu/shares/mhammelllab/www-](https://labshare.cshl.edu/shares/mhammelllab/www-data/TEtranscripts/TE_GTF/GRCh38_GENCODE_rmsk_TE.gtf.gz)
724 [data/TEtranscripts/TE_GTF/GRCh38_GENCODE_rmsk_TE.gtf.gz](https://labshare.cshl.edu/shares/mhammelllab/www-data/TEtranscripts/TE_GTF/GRCh38_GENCODE_rmsk_TE.gtf.gz)) to define repeat
725 boundaries.

726

727

728 **Gene *cis*-eQTL and L1 *trans*-eQTL analyses**

729 Gene and TE count files were loaded into R v4.2.1. Lowly expressed genes were
730 first filtered out if 323/358 European samples and 78/86 Yoruban samples did not have
731 over 0.44 counts per million (cpm) or 0.43 cpm, respectively. These fractions were
732 selected because they corresponded to expression in ~90% of samples and thus helped
733 maintain maximal statistical power by focusing on genes ubiquitously expressed across
734 each entire population. The cpm thresholds were selected because they corresponded
735 to 10 reads in the median-length library within each set of samples.

736

737 Then, counts underwent a variance stabilizing transformation (vst) using DESeq2
738 v1.36.0⁹¹. The following covariates were regressed out from vst normalized expression
739 data using the `'removeBatchEffect'` function in Limma v3.52.2⁹²: lab, population
740 category, principal components 1-2 of the pruned SNVs, biological sex, net L1/Alu copy
741 number, and EBV expression levels. Since the Yoruban samples were all from the
742 same population, the population variable was omitted in their batch correction. Here, we
743 note several things. First, EBV expression was included as a covariate because

744 heightened TE expression is often a feature of viral infections⁹³. Secondly, although
745 PEER⁷⁹ is often used to remove technical variation for *cis*-eQTL analysis, this can
746 come at the expense of correcting out genome-wide biological effects. This can be
747 problematic in some settings, such as *trans*-eQTL analysis. Thus, PEER factors were
748 not included. The batch-corrected data underwent a final inverse normal transformation
749 (INT), using the RankNorm function in the R package RNOmni v1.0.1, to obtain
750 normally distributed gene expression values.

751

752 The INT expression matrices were split into genes and L1 subfamilies, which
753 were used to identify gene *cis*-eQTLs and L1 subfamily *trans*-eQTLs in the European
754 superpopulation using MatrixEQTL v2.3⁹⁴. For gene *cis*-eQTLs, SNVs were tested for
755 association with expressed genes within 1 million base pairs. We opted to use a *trans*-
756 eQTL approach using aggregate subfamily-level TE expression since the *trans*
757 approach should allow us to identify regulators of many elements rather than one. The
758 Benjamini-Hochberg false discovery rate (FDR) was calculated in each analysis, and we
759 used the p-value corresponding to an FDR of < 5% as the threshold for eQTL
760 significance. In addition, the *cis*-eQTL and *trans*-eQTL analyses were also repeated
761 using 20 permuted expression datasets in which the sample names were scrambled,
762 and the p-value corresponding to an average empirical FDR of < 5% was used as a
763 secondary threshold. To note, we calculated the average empirical FDR at a given p-
764 value p_i by (i) counting the total number of null points with $p \leq p_i$, (ii) dividing by the
765 number of permutations, to obtain an average number of null points with $p \leq p_i$, and (iii)
766 dividing the average number of null points with $p \leq p_i$ by the number of real points with p
767 $\leq p_i$. eQTLs were called as significant if they passed the stricter of the two thresholds.
768 SNV-gene and SNV-L1 associations that were significant in the European
769 superpopulation were then targeted and tested in the Yoruban population using R's
770 built-in linear modelling functions. In this case, only the Benjamini-Hochberg FDR was
771 calculated, and significant eQTLs were called if they possessed an FDR < 5%.

772

773

774 **Defining SNV-gene-L1 trios and mediation analysis**

775 For each population, the *cis*- and *trans*-eQTL results were integrated to identify
776 SNVs associated with both gene and L1 subfamily expression. We reasoned that L1
777 expression would respond to differences in expression of *bona fide* regulators.
778 Consequently, gene expression and L1 subfamily expression associations were
779 assessed by linear regression, and the p-values from this analysis were Benjamini-
780 Hochberg FDR-corrected. Candidate SNV-gene-L1 trios were defined as those with *cis*-
781 eQTL, *trans*-eQTL, and expression regression FDRs < 5%. To identify top, index SNVs
782 in regions of linkage disequilibrium (LD), SNVs within 500 kilobases of each other with
783 an $R^2 > 0.10$ were clumped together by *trans*-eQTL p-value using PLINK v1.90b6.17.
784 Mediation analysis was carried out using the 'gmap.gpd' function in eQTLMAPT v0.1.0
785 ⁹⁵ on all candidate SNV-gene-L1 trios. Empirical p-values were calculated using 30,000
786 permutations, and Benjamini-Hochberg FDR values were calculated from empirical p-
787 values. Mediation effects were considered significant for trios with FDR < 5%.

788

789

790 **Differential expression analysis across *trans*-eQTL SNV genotypes**

791 Transcriptomic changes associated with alternating the allele of each SNV of
792 interest were evaluated using DESeq2 v1.36.0. Using the same filtered counts prepared
793 for the eQTL analysis, a linear model was constructed with the following covariates for
794 each SNV: SNV genotype in 0/1/2 format, biological sex, lab, population category,
795 principal components 1-2 of the pruned SNVs, and principal components 1-3 of the
796 pruned SVs (to account for structural variant population structure). As before, the
797 population label was omitted from the Yoruban population analysis. Significant genes
798 and TEs were those with an FDR < 5%.

799

800

801 **Functional enrichment analyses**

802 We used the Gene Set Enrichment Analysis (GSEA) paradigm as implemented
803 in the R package clusterProfiler v4.4.4 ⁹⁶. Gene Ontology, Reactome, and Hallmark
804 pathway gene sets were obtained from the R package msigdb v7.5.1, an Ensembl ID-
805 mapped collection of gene sets from the Molecular Signature Database ^{29,30}.

806 Additionally, TE subfamilies were aggregated into TE family gene sets using the TE
807 family designations specified in the TE GTF file (downloaded on February 19 2020 from
808 [https://labshare.cshl.edu/shares/mhammelllab/www-](https://labshare.cshl.edu/shares/mhammelllab/www-data/TEtranscripts/TE_GTF/GRCh38_GENCODE_rmsk_TE.gtf.gz)
809 [data/TEtranscripts/TE_GTF/GRCh38_GENCODE_rmsk_TE.gtf.gz](https://labshare.cshl.edu/shares/mhammelllab/www-data/TEtranscripts/TE_GTF/GRCh38_GENCODE_rmsk_TE.gtf.gz)) used during the
810 RNA-seq quantification step. The DESeq2 v1.36.0 Wald-statistic was used to generate
811 a combined ranked list of genes and TEs for functional enrichment analysis. All gene
812 sets with an FDR < 5% were considered significant. For plots with a single analysis, the
813 top 5 downregulated and top 5 upregulated gene sets were plotted, at most. For plots
814 with multiple analyses, shared gene sets with the desired expression patterns in each
815 individual analysis were first identified. Then, the p-values for shared gene sets were
816 combined using Fisher's method, and this meta-analysis p-value was used to rank
817 shared gene sets. Finally, the top 5 gene sets with one expression pattern and the top 5
818 gene sets with the opposite expression pattern were plotted. If there were less than 5
819 gene sets in either group, those were replaced with gene sets exhibiting the opposite
820 regulation, in order to plot 10 shared gene sets whenever possible.

821

822

823 **Cell lines and cell culture conditions.**

824 GM12878 (RRID: CVCL_7526) lymphoblastoid cells were purchased from the
825 Coriell Institute. We opted to use GM12878 as a well-characterized representative cell
826 line for candidate validation, given that (i) it is of the same cell type as the transcriptomic
827 data used here for our eQTL analysis, and (ii) its epigenomic landscape and culture
828 conditions are well-characterized as part of the ENCODE project^{39,40}.

829

830 GM12878 cells were maintained in RPMI (Corning cat. 15-040-CV) containing
831 15% FBS and 1X Penicillin-Streptomycin-Glutamine (Corning cat. 30-009-CI). Cells
832 were cultured in a humidified incubator at 37°C and 5% CO₂, subculturing cells 1:5 once
833 cells reached a density of ~10⁶ mL⁻¹. All cells used were maintained below passage 30
834 and routinely tested for mycoplasma contamination using the Plasmotest Mycoplasma
835 Detection Kit (InvivoGen).

836

837

838 **Plasmids**

839 The empty pcDNA3.1(+) backbone (Invitrogen cat. V79020) was a kind gift from
840 the lab of Dr. Changhan David Lee at the University of Southern California Leonard
841 Davis School of Gerontology. Overexpression vectors for *IL16* (CloneID OHu48263C),
842 *STARD5-FLAG* (CloneID OHu07617D), *HSD17B12-FLAG* (CloneID OHu29918D), and
843 *RNF5-FLAG* (CloneID OHu14875D) on a pcDNA3.1 backbone were purchased from
844 GenScript. Plasmid sequences were verified for accuracy using Plasmidsaurus's whole
845 plasmid sequencing service.

846

847

848 **Transfections**

849 *Escherichia coli* were cultured in LB Broth (ThermoFischer Scientific)
850 supplemented with 50 µg/mL carbenicillin to an optical density 600 (OD₆₀₀) of 2 – 4.
851 Plasmid extractions were carried out using the Nucleobond Xtra Midi Plus EF kit
852 (Macherey-Nagel) following manufacturer recommendations. Plasmids were aliquoted
853 and stored at -20°C until the time of transfection. On the day of transfection, GM12878
854 cells were collected in conical tubes, spun down (100xG, 5 minutes, room temperature),
855 resuspended in fresh media, and counted by trypan blue staining using a Countess II FL
856 automated cell counter (Thermo Fisher). The number of cells necessary for the
857 experiment were then aliquoted, spun down, and washed with Dulbecco's phosphate-
858 buffered saline (DPBS)(Corning, cat. #21-031-CV).

859

860 GM12878 cells were transfected by electroporation using the Neon Transfection
861 System (Invitrogen) with the following parameters: 1200 V, 20 ms, and 3 pulses for
862 GM12878 cells in Buffer R. Per reaction, we maintained a plasmid mass:cell number
863 ratio of 10 µg : 2*10⁶ cells. For mRNA-sequencing, 8*10⁶ GM12878 cells were
864 independently transfected for each biological replicate, with 4 replicates per
865 overexpression condition, and cultured in a T25 flask. Immediately after transfection,
866 cells were cultured in Penicillin-Streptomycin-free media for ~24 hours.

867

868 Afterwards, to promote selection of viable and healthy transfected GM12878
869 cells, we enriched for viable cells using the EasySep Dead Cell Removal (Annexin V)
870 Kit (STEMCELL Technologies) before seeding 2×10^6 live cells in the same media used
871 for cell maintenance. After another 24 hours, cell viability was measured by trypan blue
872 staining on a Countess automated cell counter and cells were spun down (100xG, 5
873 min, room temperature) and lysed in TRIzol Reagent (Invitrogen) for downstream total
874 RNA isolation (see below).

875

876

877 **Recombinant human IL16 (rhIL16) peptide treatment**

878 Human rIL16 was obtained from PeproTech (cat. #200-16) and resuspended in
879 0.1% bovine serum albumin (BSA) solution (Akron, cat. #AK8917-0100). GM12878 cells
880 were seeded at a concentration of 500,000 live cells per mL of media on 6-well
881 suspension plates with 3 independent replicates per condition. Cells were exposed to 0,
882 24, or 48 hours of 100 ng mL^{-1} of rhIL16. To replace or exchange media 24 hours after
883 seeding, cells were transferred to conical tubes, spun down (100xG, 5 min, room
884 temperature), resuspended in 5 mL of the appropriate media, and transferred back to 6-
885 well suspension plates. After 48 hours, cell viability was measured by trypan blue
886 staining and cells were spun down (100xG, 5 min, room temperature) and lysed in
887 TRIzol Reagent (Invitrogen).

888

889

890 **RNA extractions and mRNA sequencing**

891 RNA was extracted using the Direct-zol RNA Miniprep kit (Zymo Research)
892 following manufacturer recommendations. The integrity of RNA samples was evaluated
893 using an Agilent High Sensitivity RNA ScreenTape assay (Agilent Technologies),
894 ensuring that all samples had a minimum eRIN score of 8 before downstream
895 processing. We then submitted total RNA samples to Novogene (Sacramento,
896 California) for mRNA library preparation and sequencing on the NovaSeq 6000 platform
897 as paired-end 150 bp reads.

898

899

900 **Analysis of overexpression and rhIL16 exposure mRNA-seq**

901 mRNA-seq reads were trimmed, mapped, and quantified like for the eQTL
902 analysis, except for the overexpression sample data. For this data, one modification
903 was made: the EBV-inclusive reference genome was further modified to include the
904 pcDNA3.1 sequence as an additional contig. Lowly expressed genes were filtered using
905 a cpm threshold as in the eQTL processing, but that cpm threshold had to be satisfied
906 by as many samples as the size of the smallest biological group. For the overexpression
907 data, surrogate variables were estimated with the 'svaseq' function⁸⁰ in the R package
908 'sva' v3.44.9, and they were regressed out from the raw read counts using the
909 'removeBatchEffect' function in the R package Limma v3.52.2. DESeq2 was used to
910 identify significantly (FDR < 5%) differentially expressed genes and TEs between
911 groups. Functional enrichment analysis was carried out as previously described.

912

913

914 **PheWAS analysis**

915 To gather the known associated traits for the 499 TE-related SNVs, we used
916 Open Targets Genetics (<https://genetics.opentargets.org/>), a database of GWAS
917 summary statistics⁹⁷. First, we queried the database using the 499 TE-related SNVs
918 and collected traits that were directly associated (with $P < 5 \times 10^{-8}$) with the SNVs, as well
919 as traits associated with lead variants that were in linkage disequilibrium (LD) with the
920 queried SNPs (with $R^2 > 0.6$). For age-related traits (ARTs), we used the
921 comprehensive list of 365 Medical Subject Headings (MeSH) terms reported by⁹⁸
922 (downloaded from <https://github.com/kisudsoe/Age-related-traits>). To identify known
923 age-related traits, the known associated traits were translated into the equivalent MeSH
924 terms using the method described by⁹⁸. Then, the MeSH-translated known associated
925 traits for the 499 TE-related SNVs were filtered by the MeSH terms for age-related
926 traits.

927

928 As a parallel approach, we mapped the RsIDs for all SNVs used during the eQTL
929 analyses to their corresponding bi-allelic Open Targets variant IDs, when available. The

930 variant IDs corresponding to L1 *trans*-eQTL SNVs were extracted, and 500 different
931 equal-length combinations of random SNVs were generated. Next, we queried the Open
932 Targets database using the lists of L1-associated and random SNVs and collected the
933 associated traits (with $P < 5 \times 10^{-8}$). Importantly, the database assigns traits to broader
934 categories, including 14 disease categories that we considered age-related. We
935 counted the number of L1-associated or random SNVs mapping to each category, and
936 we used the random SNV counts to generate an empirical cumulative distribution
937 function (ecdf) for each category. We calculated enrichment p-values using the formula
938 $p = 1 - \text{ecdf}(\text{mapped eQTLs})$ and then Benjamini-Hochberg FDR-corrected all p-values.
939 An enrichment score (ES) was also calculated for each category using the formula $\text{ES} =$
940 $\text{number of mapped L1 eQTLs} / \text{median number of randomly mapping SNVs}$. Categories
941 with an $\text{ES} > 1$ and $\text{FDR} < 0.05$ were considered significantly enriched.

942

943

944 **Mouse husbandry**

945 All animals were treated and housed in accordance with the Guide for Care and
946 Use of Laboratory Animals. All experimental procedures were approved by the
947 University of Southern California's Institutional Animal Care and Use Committee
948 (IACUC) and are in accordance with institutional and national guidelines. Samples were
949 derived from animals on approved IACUC protocol #20770.

950

951

952 **Quantification of mouse serum IL16 by ELISA**

953 Serum was collected from male and female C57BL/6JNia mice (4-6 and 20-24
954 months old) obtained from the National Institute on Aging (NIA) colony at Charles
955 Rivers. All animals were euthanized between 8-11 am in a "snaking order" across all
956 groups to minimize batch-processing confounds due to circadian processes. All animals
957 were euthanized by CO₂ asphyxiation followed by cervical dislocation. Circulating IL16
958 levels were quantitatively evaluated from mouse serum by enzyme-linked
959 immunosorbent assay (ELISA). Serum was diluted 1/10 before quantifying IL16
960 concentrations using Abcam's Mouse IL-16 ELISA Kit (ab201282) in accordance with

961 manufacturer instructions. Technical replicates from the same sample were averaged to
962 one value before statistical analysis and plotting. P-values across age within each sex
963 were calculated using a non-parametric 2-sided Wilcoxon test, and p-values from each
964 sex-specific analysis were combined using Fisher's method.

965

966

967 **Data availability**

968 New sequencing data generated in this study is accessible through the
969 Sequence Read Archive (SRA) under BioProject PRJNA937306. All code is available
970 on the Benayoun lab GitHub (https://github.com/BenayounLaboratory/TE-eQTL_LCLs).
971 Analyses were conducted using R version 4.2.1. Code was re-run independently on R
972 version 4.3.0 to check for reproducibility.

973

974

975

976 **Competing interest statement**

977 The authors have no conflict of interest.

978

979 **Acknowledgements**

980 Some panels were created with BioRender.com. We would like to thank Prof.
981 Rachel Brem for her feedback and insights on the eQTL analyses. We would also like to
982 thank Dr. Minhoo Kim for her feedback on the manuscript.

983 This work was supported by NSF Graduate Research Fellowship Program (NSF
984 GRFP) DGE-1842487 (J.I.B.), NIA T32 AG052374 (J.I.B.), the University of Southern
985 California with a Provost Fellowship (J.I.B.), NIA R25 AG076400 (C.R.M.), and NIGMS
986 R35 GM142395 (to B.A.B).

987

988 **Author contributions**

989 J.I.B. and B.A.B designed the study. J.I.B., L.Z., and S.K. performed data
990 analyses, with guidance from Y.S. and B.A.B. J.I.B. and C.R.M. carried out
991 experiments. J.I.B., B.A.B., S.K., and Y.S. wrote the manuscript. All authors contributed
992 to the editing of the manuscript.

993

994

995 References

- 996 1. Lander, E.S., Linton, L.M., Birren, B., Nusbaum, C., Zody, M.C., Baldwin, J.,
997 Devon, K., Dewar, K., Doyle, M., FitzHugh, W., et al. (2001). Initial sequencing
998 and analysis of the human genome. *Nature* *409*, 860-921. [10.1038/35057062](https://doi.org/10.1038/35057062).
- 999 2. Venter, J.C., Adams, M.D., Myers, E.W., Li, P.W., Mural, R.J., Sutton, G.G.,
1000 Smith, H.O., Yandell, M., Evans, C.A., Holt, R.A., et al. (2001). The Sequence of
1001 the Human Genome. *Science* *291*, 1304-1351. doi:10.1126/science.1058040.
- 1002 3. Brouha, B., Schustak, J., Badge, R.M., Lutz-Prigge, S., Farley, A.H., Moran, J.V.,
1003 and Kazazian, H.H. (2003). Hot L1s account for the bulk of retrotransposition in
1004 the human population. *Proceedings of the National Academy of Sciences* *100*,
1005 5280-5285. doi:10.1073/pnas.0831042100.
- 1006 4. Moran, J.V., Holmes, S.E., Naas, T.P., DeBerardinis, R.J., Boeke, J.D., and
1007 Kazazian, H.H., Jr. (1996). High Frequency Retrotransposition in Cultured
1008 Mammalian Cells. *Cell* *87*, 917-927. [10.1016/S0092-8674\(00\)81998-4](https://doi.org/10.1016/S0092-8674(00)81998-4).
- 1009 5. Bravo, J.I., Nozownik, S., Danthi, P.S., and Benayoun, B.A. (2020).
1010 Transposable elements, circular RNAs and mitochondrial transcription in age-
1011 related genomic regulation. *Development* *147*. [10.1242/dev.175786](https://doi.org/10.1242/dev.175786).
- 1012 6. Della Valle, F., Reddy, P., Yamamoto, M., Liu, P., Saera-Vila, A., Bensaddek, D.,
1013 Zhang, H., Prieto Martinez, J., Abassi, L., Celii, M., et al. (2022). *LINE-1* RNA
1014 causes heterochromatin erosion and is a target for amelioration of senescent
1015 phenotypes in progeroid syndromes. *Science Translational Medicine* *14*,
1016 eabl6057. doi:10.1126/scitranslmed.abl6057.
- 1017 7. Simon, M., Van Meter, M., Ablueva, J., Ke, Z., Gonzalez, R.S., Taguchi, T., De
1018 Cecco, M., Leonova, K.I., Kogan, V., Helfand, S.L., et al. (2019). LINE1
1019 Derepression in Aged Wild-Type and SIRT6-Deficient Mice Drives Inflammation.
1020 *Cell Metabolism* *29*, 871-885.e875. [10.1016/j.cmet.2019.02.014](https://doi.org/10.1016/j.cmet.2019.02.014).
- 1021 8. Zhao, Y., Oreskovic, E., Zhang, Q., Lu, Q., Gilman, A., Lin, Y.S., He, J., Zheng,
1022 Z., Lu, J.Y., Lee, J., et al. (2021). Transposon-triggered innate immune response
1023 confers cancer resistance to the blind mole rat. *Nature Immunology* *22*, 1219-
1024 1230. [10.1038/s41590-021-01027-8](https://doi.org/10.1038/s41590-021-01027-8).

- 1025 9. Zhao, H., Ji, Q., Wu, Z., Wang, S., Ren, J., Yan, K., Wang, Z., Hu, J., Chu, Q.,
1026 Hu, H., et al. (2022). Destabilizing heterochromatin by APOE mediates
1027 senescence. *Nature Aging* 2, 303-316. [10.1038/s43587-022-00186-z](https://doi.org/10.1038/s43587-022-00186-z).
- 1028 10. Liu, E.Y., Russ, J., Cali, C.P., Phan, J.M., Amlie-Wolf, A., and Lee, E.B. (2019).
1029 Loss of Nuclear TDP-43 Is Associated with Decondensation of LINE
1030 Retrotransposons. *Cell Reports* 27, 1409-1421.e1406.
1031 [10.1016/j.celrep.2019.04.003](https://doi.org/10.1016/j.celrep.2019.04.003).
- 1032 11. De Cecco, M., Criscione, S.W., Peterson, A.L., Neretti, N., Sedivy, J.M., and
1033 Kreiling, J.A. (2013). Transposable elements become active and mobile in the
1034 genomes of aging mammalian somatic tissues. *Aging (Albany NY)* 5, 867-883.
1035 [10.18632/aging.100621](https://doi.org/10.18632/aging.100621).
- 1036 12. De Cecco, M., Criscione, S.W., Peckham, E.J., Hillenmeyer, S., Hamm, E.A.,
1037 Manivannan, J., Peterson, A.L., Kreiling, J.A., Neretti, N., and Sedivy, J.M.
1038 (2013). Genomes of replicatively senescent cells undergo global epigenetic
1039 changes leading to gene silencing and activation of transposable elements.
1040 *Aging Cell* 12, 247-256. <https://doi.org/10.1111/acer.12047>.
- 1041 13. Campisi, J. (2013). Aging, Cellular Senescence, and Cancer. *Annual Review of*
1042 *Physiology* 75, 685-705. [10.1146/annurev-physiol-030212-183653](https://doi.org/10.1146/annurev-physiol-030212-183653).
- 1043 14. Franceschi, C., Garagnani, P., Parini, P., Giuliani, C., and Santoro, A. (2018).
1044 Inflammaging: a new immune–metabolic viewpoint for age-related diseases.
1045 *Nature Reviews Endocrinology* 14, 576-590. [10.1038/s41574-018-0059-4](https://doi.org/10.1038/s41574-018-0059-4).
- 1046 15. De Cecco, M., Ito, T., Petrashen, A.P., Elias, A.E., Skvir, N.J., Criscione, S.W.,
1047 Caligiana, A., Broccoli, G., Adney, E.M., Boeke, J.D., et al. (2019). L1 drives IFN
1048 in senescent cells and promotes age-associated inflammation. *Nature* 566, 73-
1049 78. [10.1038/s41586-018-0784-9](https://doi.org/10.1038/s41586-018-0784-9).
- 1050 16. Rodriguez-Martin, B., Alvarez, E.G., Baez-Ortega, A., Zamora, J., Supek, F.,
1051 Demeulemeester, J., Santamarina, M., Ju, Y.S., Temes, J., Garcia-Souto, D., et
1052 al. (2020). Pan-cancer analysis of whole genomes identifies driver
1053 rearrangements promoted by LINE-1 retrotransposition. *Nature Genetics* 52,
1054 306-319. [10.1038/s41588-019-0562-0](https://doi.org/10.1038/s41588-019-0562-0).

- 1055 17. Flasch, D.A., Chen, X., Ju, B., Li, X., Dalton, J., Mulder, H.L., Easton, J., Wang,
1056 L., Baker, S.J., Chiang, J., and Zhang, J. (2022). Somatic LINE-1 promoter
1057 acquisition drives oncogenic FOXR2 activation in pediatric brain tumor. *Acta*
1058 *Neuropathologica* 143, 605-607. 10.1007/s00401-022-02420-9.
- 1059 18. Levin, H.L., and Moran, J.V. (2011). Dynamic interactions between transposable
1060 elements and their hosts. *Nature Reviews Genetics* 12, 615-627.
1061 10.1038/nrg3030.
- 1062 19. Rebollo, R., Romanish, M.T., and Mager, D.L. (2012). Transposable Elements:
1063 An Abundant and Natural Source of Regulatory Sequences for Host Genes.
1064 *Annual Review of Genetics* 46, 21-42. 10.1146/annurev-genet-110711-155621.
- 1065 20. Liu, N., Lee, C.H., Swigut, T., Grow, E., Gu, B., Bassik, M.C., and Wysocka, J.
1066 (2018). Selective silencing of euchromatic L1s revealed by genome-wide screens
1067 for L1 regulators. *Nature* 553, 228-232. 10.1038/nature25179.
- 1068 21. Chung, N., Jonaid, G.M., Quinton, S., Ross, A., Sexton, C.E., Alberto, A.,
1069 Clymer, C., Churchill, D., Navarro Leija, O., and Han, M.V. (2019). Transcriptome
1070 analyses of tumor-adjacent somatic tissues reveal genes co-expressed with
1071 transposable elements. *Mobile DNA* 10, 39. 10.1186/s13100-019-0180-5.
- 1072 22. Auton, A., Abecasis, G.R., Altshuler, D.M., Durbin, R.M., Abecasis, G.R.,
1073 Bentley, D.R., Chakravarti, A., Clark, A.G., Donnelly, P., Eichler, E.E., et al.
1074 (2015). A global reference for human genetic variation. *Nature* 526, 68-74.
1075 10.1038/nature15393.
- 1076 23. Sudmant, P.H., Rausch, T., Gardner, E.J., Handsaker, R.E., Abyzov, A.,
1077 Huddleston, J., Zhang, Y., Ye, K., Jun, G., Hsi-Yang Fritz, M., et al. (2015). An
1078 integrated map of structural variation in 2,504 human genomes. *Nature* 526, 75-
1079 81. 10.1038/nature15394.
- 1080 24. Sie, L., Loong, S., and Tan, E.K. (2009). Utility of lymphoblastoid cell lines.
1081 *Journal of Neuroscience Research* 87, 1953-1959.
1082 <https://doi.org/10.1002/jnr.22000>.
- 1083 25. Hussain, T., and Mulherkar, R. (2012). Lymphoblastoid Cell lines: a Continuous
1084 in Vitro Source of Cells to Study Carcinogen Sensitivity and DNA Repair. *Int J*
1085 *Mol Cell Med* 1, 75-87.

- 1086 26. Lappalainen, T., Sammeth, M., Friedländer, M.R., 't Hoen, P.A.C., Monlong, J.,
1087 Rivas, M.A., González-Porta, M., Kurbatova, N., Griebel, T., Ferreira, P.G., et al.
1088 (2013). Transcriptome and genome sequencing uncovers functional variation in
1089 humans. *Nature* *501*, 506-511. 10.1038/nature12531.
- 1090 27. Jin, Y., Tam, O.H., Paniagua, E., and Hammell, M. (2015). Tetrascripts: a
1091 package for including transposable elements in differential expression analysis of
1092 RNA-seq datasets. *Bioinformatics* *31*, 3593-3599. 10.1093/bioinformatics/btv422.
- 1093 28. Williams, T.M. (2001). Human Leukocyte Antigen Gene Polymorphism and the
1094 Histocompatibility Laboratory. *The Journal of Molecular Diagnostics* *3*, 98-104.
1095 10.1016/S1525-1578(10)60658-7.
- 1096 29. Subramanian, A., Tamayo, P., Mootha, V.K., Mukherjee, S., Ebert, B.L., Gillette,
1097 M.A., Paulovich, A., Pomeroy, S.L., Golub, T.R., Lander, E.S., and Mesirov, J.P.
1098 (2005). Gene set enrichment analysis: A knowledge-based approach for
1099 interpreting genome-wide expression profiles. *Proceedings of the National*
1100 *Academy of Sciences* *102*, 15545-15550. doi:10.1073/pnas.0506580102.
- 1101 30. Liberzon, A., Birger, C., Thorvaldsdóttir, H., Ghandi, M., Mesirov, J.P., and
1102 Tamayo, P. (2015). The Molecular Signatures Database (MSigDB) hallmark gene
1103 set collection. *Cell Syst* *1*, 417-425. 10.1016/j.cels.2015.12.004.
- 1104 31. Marasca, F., Sinha, S., Vadalà, R., Polimeni, B., Ranzani, V., Paraboschi, E.M.,
1105 Burattin, F.V., Ghilotti, M., Crosti, M., Negri, M.L., et al. (2022). LINE1 are spliced
1106 in non-canonical transcript variants to regulate T cell quiescence and exhaustion.
1107 *Nature Genetics* *54*, 180-193. 10.1038/s41588-021-00989-7.
- 1108 32. Wahl, D., Cavalier, A.N., Smith, M., Seals, D.R., and LaRocca, T.J. (2020).
1109 Healthy Aging Interventions Reduce Repetitive Element Transcripts. *The*
1110 *Journals of Gerontology: Series A* *76*, 805-810. 10.1093/gerona/glaa302.
- 1111 33. Sampathkumar, N.K., Bravo, J.I., Chen, Y., Danthi, P.S., Donahue, E.K., Lai,
1112 R.W., Lu, R., Randall, L.T., Vinson, N., and Benayoun, B.A. (2020). Widespread
1113 sex dimorphism in aging and age-related diseases. *Hum Genet* *139*, 333-356.
1114 10.1007/s00439-019-02082-w.
- 1115 34. Baeken, M.W., Moosmann, B., and Hajieva, P. (2020). Retrotransposon
1116 activation by distressed mitochondria in neurons. *Biochemical and Biophysical*

- 1147 43. Theodore, A.C., Center, D.M., Nicoll, J., Fine, G., Kornfeld, H., and Cruikshank,
1148 W.W. (1996). CD4 ligand IL-16 inhibits the mixed lymphocyte reaction. *J*
1149 *Immunol* *157*, 1958-1964.
- 1150 44. Cruikshank, W.W., Lim, K., Theodore, A.C., Cook, J., Fine, G., Weller, P.F., and
1151 Center, D.M. (1996). IL-16 inhibition of CD3-dependent lymphocyte activation
1152 and proliferation. *J Immunol* *157*, 5240-5248.
- 1153 45. Center, D.M., Kornfeld, H., and Cruikshank, W.W. (1996). Interleukin 16 and its
1154 function as a CD4 ligand. *Immunol Today* *17*, 476-481. 10.1016/0167-
1155 5699(96)10052-i.
- 1156 46. Wilson, K.C., Center, D.M., and Cruikshank, W.W. (2004). Mini ReviewThe Effect
1157 of Interleukin-16 and its Precursor on T Lymphocyte Activation and Growth.
1158 *Growth Factors* *22*, 97-104. 10.1080/08977190410001704679.
- 1159 47. Huang, Y., Du, K.L., Guo, P.Y., Zhao, R.M., Wang, B., Zhao, X.L., and Zhang,
1160 C.Q. (2019). IL-16 regulates macrophage polarization as a target gene of mir-
1161 145-3p. *Mol Immunol* *107*, 1-9. 10.1016/j.molimm.2018.12.027.
- 1162 48. Rodriguez-Agudo, D., Malacrida, L., Kakiyama, G., Sparrer, T., Fortes, C.,
1163 Maceyka, M., Subler, M.A., Windle, J.J., Gratton, E., Pandak, W.M., and Gil, G.
1164 (2019). StarD5: an ER stress protein regulates plasma membrane and
1165 intracellular cholesterol homeostasis. *Journal of Lipid Research* *60*, 1087-1098.
1166 10.1194/jlr.M091967.
- 1167 49. Rodriguez-Agudo, D., Calderon-Dominguez, M., Medina, M.A., Ren, S., Gil, G.,
1168 and Pandak, W.M. (2012). ER stress increases StarD5 expression by stabilizing
1169 its mRNA and leads to relocalization of its protein from the nucleus to the
1170 membranes. *J Lipid Res* *53*, 2708-2715. 10.1194/jlr.M031997.
- 1171 50. Soccio, R.E., Adams, R.M., Maxwell, K.N., and Breslow, J.L. (2005). Differential
1172 Gene Regulation of StarD4 and StarD5 Cholesterol Transfer Proteins:
1173 ACTIVATION OF StarD4 BY STEROL REGULATORY ELEMENT-BINDING
1174 PROTEIN-2 AND StarD5 BY ENDOPLASMIC RETICULUM STRESS *. *Journal*
1175 *of Biological Chemistry* *280*, 19410-19418. 10.1074/jbc.M501778200.
- 1176 51. Luu-The, V., Tremblay, P., and Labrie, F. (2006). Characterization of type 12
1177 17beta-hydroxysteroid dehydrogenase, an isoform of type 3 17beta-

- 1178 hydroxysteroid dehydrogenase responsible for estradiol formation in women. *Mol*
1179 *Endocrinol* *20*, 437-443. 10.1210/me.2005-0058.
- 1180 52. Heikelä, H., Ruohonen, S.T., Adam, M., Viitanen, R., Liljenbäck, H., Eskola, O.,
1181 Gabriel, M., Mairinoja, L., Pessia, A., Velagapudi, V., et al. (2020).
1182 Hydroxysteroid (17 β) dehydrogenase 12 is essential for metabolic homeostasis
1183 in adult mice. *Am J Physiol Endocrinol Metab* *319*, E494-e508.
1184 10.1152/ajpendo.00042.2020.
- 1185 53. Nagasaki, S., Miki, Y., Akahira, J., Suzuki, T., and Sasano, H. (2009).
1186 Transcriptional regulation of 17beta-hydroxysteroid dehydrogenase type 12 by
1187 SREBP-1. *Mol Cell Endocrinol* *307*, 163-168. 10.1016/j.mce.2009.04.002.
- 1188 54. Didier, C., Broday, L., Bhoumik, A., Israeli, S., Takahashi, S., Nakayama, K.,
1189 Thomas, S.M., Turner, C.E., Henderson, S., Sabe, H., and Ronai, Z.e. (2003).
1190 RNF5, a RING Finger Protein That Regulates Cell Motility by Targeting Paxillin
1191 Ubiquitination and Altered Localization. *Molecular and Cellular Biology* *23*, 5331-
1192 5345. 10.1128/MCB.23.15.5331-5345.2003.
- 1193 55. Tcherpakov, M., Delaunay, A., Toth, J., Kadoya, T., Petroski, M.D., and Ronai,
1194 Z.e.A. (2009). Regulation of Endoplasmic Reticulum-associated Degradation by
1195 RNF5-dependent Ubiquitination of JNK-associated Membrane Protein (JAMP) *.
1196 *Journal of Biological Chemistry* *284*, 12099-12109. 10.1074/jbc.M808222200.
- 1197 56. Zhong, B., Zhang, Y., Tan, B., Liu, T.T., Wang, Y.Y., and Shu, H.B. (2010). The
1198 E3 ubiquitin ligase RNF5 targets virus-induced signaling adaptor for
1199 ubiquitination and degradation. *J Immunol* *184*, 6249-6255.
1200 10.4049/jimmunol.0903748.
- 1201 57. Zhong, B., Zhang, L., Lei, C., Li, Y., Mao, A.-P., Yang, Y., Wang, Y.-Y., Zhang,
1202 X.-L., and Shu, H.-B. (2009). The Ubiquitin Ligase RNF5 Regulates Antiviral
1203 Responses by Mediating Degradation of the Adaptor Protein MITA. *Immunity* *30*,
1204 397-407. <https://doi.org/10.1016/j.immuni.2009.01.008>.
- 1205 58. Lai, R.W., Lu, R., Danthi, P.S., Bravo, J.I., Goumba, A., Sampathkumar, N.K.,
1206 and Benayoun, B.A. (2019). Multi-level remodeling of transcriptional landscapes
1207 in aging and longevity. *BMB Rep* *52*, 86-108. 10.5483/BMBRep.2019.52.1.296.

- 1208 59. Sato, S., Gillette, M., de Santiago, P.R., Kuhn, E., Burgess, M., Doucette, K.,
1209 Feng, Y., Mendez-Dorantes, C., Ippoliti, P.J., Hobday, S., et al. (2023). LINE-1
1210 ORF1p as a candidate biomarker in high grade serous ovarian carcinoma.
1211 *Scientific Reports* 13, 1537. 10.1038/s41598-023-28840-5.
- 1212 60. Rodić, N., Sharma, R., Sharma, R., Zampella, J., Dai, L., Taylor, M.S., Hruban,
1213 R.H., Iacobuzio-Donahue, C.A., Maitra, A., Torbenson, M.S., et al. (2014). Long
1214 Interspersed Element-1 Protein Expression Is a Hallmark of Many Human
1215 Cancers. *The American Journal of Pathology* 184, 1280-1286.
1216 10.1016/j.ajpath.2014.01.007.
- 1217 61. Lindholm, H.T., Chen, R., and De Carvalho, D.D. (2023). Endogenous
1218 retroelements as alarms for disruptions to cellular homeostasis. *Trends in Cancer*
1219 9, 55-68. 10.1016/j.trecan.2022.09.001.
- 1220 62. Jeck, W.R., Siebold, A.P., and Sharpless, N.E. (2012). Review: a meta-analysis
1221 of GWAS and age-associated diseases. *Aging Cell* 11, 727-731.
1222 <https://doi.org/10.1111/j.1474-9726.2012.00871.x>.
- 1223 63. Ramirez, J., Bitterman, P., Basu, S., and Barua, A. (2022). Changes in IL-16
1224 Expression in the Ovary during Aging and Its Potential Consequences to Ovarian
1225 Pathology. *J Immunol Res* 2022, 2870389. 10.1155/2022/2870389.
- 1226 64. Lonsdale, J., Thomas, J., Salvatore, M., Phillips, R., Lo, E., Shad, S., Hasz, R.,
1227 Walters, G., Garcia, F., Young, N., et al. (2013). The Genotype-Tissue
1228 Expression (GTEx) project. *Nature Genetics* 45, 580-585. 10.1038/ng.2653.
- 1229 65. Carithers, L.J., Ardlie, K., Barcus, M., Branton, P.A., Britton, A., Buia, S.A.,
1230 Compton, C.C., DeLuca, D.S., Peter-Demchok, J., Gelfand, E.T., et al. (2015). A
1231 Novel Approach to High-Quality Postmortem Tissue Procurement: The GTEx
1232 Project. *Biopreservation and Biobanking* 13, 311-319. 10.1089/bio.2015.0032.
- 1233 66. Streeter, I., Harrison, P.W., Faulconbridge, A., The HipSci Consortium, Flicek, P.,
1234 Parkinson, H., and Clarke, L. (2016). The human-induced pluripotent stem cell
1235 initiative—data resources for cellular genetics. *Nucleic Acids Research* 45, D691-
1236 D697. 10.1093/nar/gkw928.
- 1237 67. Chick, J.M., Munger, S.C., Simecek, P., Huttlin, E.L., Choi, K., Gatti, D.M.,
1238 Raghupathy, N., Svenson, K.L., Churchill, G.A., and Gygi, S.P. (2016). Defining

- 1239 the consequences of genetic variation on a proteome-wide scale. *Nature* *534*,
1240 500-505. [10.1038/nature18270](https://doi.org/10.1038/nature18270).
- 1241 68. Baier, M., Werner, A., Bannert, N., Metzner, K., and Kurth, R. (1995). HIV
1242 suppression by interleukin-16. *Nature* *378*, 563. [10.1038/378563a0](https://doi.org/10.1038/378563a0).
- 1243 69. Zhou, P., Goldstein, S., Devadas, K., Tewari, D., and Notkins, A.L. (1997).
1244 Human CD4+ cells transfected with IL-16 cDNA are resistant to HIV-1 infection:
1245 inhibition of mRNA expression. *Nat Med* *3*, 659-664. [10.1038/nm0697-659](https://doi.org/10.1038/nm0697-659).
- 1246 70. Idziorek, T., Khalife, J., Billaut-Mulot, O., Hermann, E., Aumercier, M., Mouton,
1247 Y., Capron, A., and Bahr, G.M. (1998). Recombinant human IL-16 inhibits HIV-1
1248 replication and protects against activation-induced cell death (AICD). *Clin Exp*
1249 *Immunol* *112*, 84-91. [10.1046/j.1365-2249.1998.00550.x](https://doi.org/10.1046/j.1365-2249.1998.00550.x).
- 1250 71. Jia, R., Jiang, C., Li, L., Huang, C., Lu, L., Xu, M., Xu, J., and Liang, X. (2021).
1251 Interleukin 16 Enhances the Host Susceptibility to Influenza A Virus Infection.
1252 *Frontiers in Microbiology* *12*. [10.3389/fmicb.2021.736449](https://doi.org/10.3389/fmicb.2021.736449).
- 1253 72. Liu, S., Lei, Z., Li, J., Wang, L., Jia, R., Liu, Z., Jiang, C., Gao, Y., Liu, M., Kuang,
1254 L., et al. (2020). Interleukin 16 contributes to gammaherpesvirus pathogenesis by
1255 inhibiting viral reactivation. *PLoS Pathog* *16*, e1008701.
1256 [10.1371/journal.ppat.1008701](https://doi.org/10.1371/journal.ppat.1008701).
- 1257 73. Watanabe, T., Watanabe, S., and Kawaoka, Y. (2010). Cellular Networks
1258 Involved in the Influenza Virus Life Cycle. *Cell Host & Microbe* *7*, 427-439.
1259 [10.1016/j.chom.2010.05.008](https://doi.org/10.1016/j.chom.2010.05.008).
- 1260 74. Germain, M.A., Chatel-Chaix, L., Gagné, B., Bonneil, É., Thibault, P.,
1261 Pradezynski, F., de Chasse, B., Meyniel-Schicklin, L., Lotteau, V., Baril, M., and
1262 Lamarre, D. (2014). Elucidating novel hepatitis C virus-host interactions using
1263 combined mass spectrometry and functional genomics approaches. *Mol Cell*
1264 *Proteomics* *13*, 184-203. [10.1074/mcp.M113.030155](https://doi.org/10.1074/mcp.M113.030155).
- 1265 75. Mohamed, B., Mazeaud, C., Baril, M., Poirier, D., Sow, A.A., Chatel-Chaix, L.,
1266 Titorenko, V., and Lamarre, D. (2020). Very-long-chain fatty acid metabolic
1267 capacity of 17-beta-hydroxysteroid dehydrogenase type 12 (HSD17B12)
1268 promotes replication of hepatitis C virus and related flaviviruses. *Scientific*
1269 *Reports* *10*, 4040. [10.1038/s41598-020-61051-w](https://doi.org/10.1038/s41598-020-61051-w).

- 1270 76. Feng, K., Min, Y.-Q., Sun, X., Deng, F., Li, P., Wang, H., and Ning, Y.-J. (2021).
1271 Interactome profiling reveals interaction of SARS-CoV-2 NSP13 with host factor
1272 STAT1 to suppress interferon signaling. *Journal of Molecular Cell Biology* 13,
1273 760-762. [10.1093/jmcb/mjab068](https://doi.org/10.1093/jmcb/mjab068).
- 1274 77. Yuan, Z., Hu, B., Xiao, H., Tan, X., Li, Y., Tang, K., Zhang, Y., Cai, K., and Ding,
1275 B. (2022). The E3 Ubiquitin Ligase RNF5 Facilitates SARS-CoV-2 Membrane
1276 Protein-Mediated Virion Release. *mBio* 13, e03168-03121.
1277 [doi:10.1128/mbio.03168-21](https://doi.org/10.1128/mbio.03168-21).
- 1278 78. Li, Z., Hao, P., Zhao, Z., Gao, W., Huan, C., Li, L., Chen, X., Wang, H., Jin, N.,
1279 Luo, Z.-Q., et al. (2023). The E3 ligase RNF5 restricts SARS-CoV-2 replication
1280 by targeting its envelope protein for degradation. *Signal Transduction and*
1281 *Targeted Therapy* 8, 53. [10.1038/s41392-023-01335-5](https://doi.org/10.1038/s41392-023-01335-5).
- 1282 79. Stegle, O., Parts, L., Piipari, M., Winn, J., and Durbin, R. (2012). Using
1283 probabilistic estimation of expression residuals (PEER) to obtain increased
1284 power and interpretability of gene expression analyses. *Nat Protoc* 7, 500-507.
1285 [10.1038/nprot.2011.457](https://doi.org/10.1038/nprot.2011.457).
- 1286 80. Leek, J.T. (2014). svaseq: removing batch effects and other unwanted noise from
1287 sequencing data. *Nucleic Acids Research* 42, e161-e161. [10.1093/nar/gku864](https://doi.org/10.1093/nar/gku864).
- 1288 81. Savytska, N., Heutink, P., and Bansal, V. (2022). Transcription start site signal
1289 profiling improves transposable element RNA expression analysis at locus-level.
1290 *Frontiers in Genetics* 13. [10.3389/fgene.2022.1026847](https://doi.org/10.3389/fgene.2022.1026847).
- 1291 82. Danecek, P., Bonfield, J.K., Liddle, J., Marshall, J., Ohan, V., Pollard, M.O.,
1292 Whitwham, A., Keane, T., McCarthy, S.A., Davies, R.M., and Li, H. (2021).
1293 Twelve years of SAMtools and BCFtools. *GigaScience* 10.
1294 [10.1093/gigascience/giab008](https://doi.org/10.1093/gigascience/giab008).
- 1295 83. Danecek, P., Auton, A., Abecasis, G., Albers, C.A., Banks, E., DePristo, M.A.,
1296 Handsaker, R.E., Lunter, G., Marth, G.T., Sherry, S.T., et al. (2011). The variant
1297 call format and VCFtools. *Bioinformatics* 27, 2156-2158.
1298 [10.1093/bioinformatics/btr330](https://doi.org/10.1093/bioinformatics/btr330).

- 1299 84. Gao, F., Chang, D., Biddanda, A., Ma, L., Guo, Y., Zhou, Z., and Keinan, A.
1300 (2015). XWAS: A Software Toolset for Genetic Data Analysis and Association
1301 Studies of the X Chromosome. *J Hered* 106, 666-671. 10.1093/jhered/esv059.
- 1302 85. Keur, N., Ricaño-Ponce, I., Kumar, V., and Matzaraki, V. (2022). A systematic
1303 review of analytical methods used in genetic association analysis of the X-
1304 chromosome. *Briefings in Bioinformatics* 23. 10.1093/bib/bbac287.
- 1305 86. Purcell, S., Neale, B., Todd-Brown, K., Thomas, L., Ferreira, M.A.R., Bender, D.,
1306 Maller, J., Sklar, P., de Bakker, P.I.W., Daly, M.J., and Sham, P.C. (2007).
1307 PLINK: A Tool Set for Whole-Genome Association and Population-Based
1308 Linkage Analyses. *The American Journal of Human Genetics* 81, 559-575.
1309 10.1086/519795.
- 1310 87. Ahl, V., Keller, H., Schmidt, S., and Weichenrieder, O. (2015). Retrotransposition
1311 and Crystal Structure of an Alu RNP in the Ribosome-Stalling Conformation.
1312 *Molecular Cell* 60, 715-727. <https://doi.org/10.1016/j.molcel.2015.10.003>.
- 1313 88. Chen, S., Zhou, Y., Chen, Y., and Gu, J. (2018). fastp: an ultra-fast all-in-one
1314 FASTQ preprocessor. *Bioinformatics* 34, i884-i890.
1315 10.1093/bioinformatics/bty560.
- 1316 89. Frankish, A., Diekhans, M., Ferreira, A.-M., Johnson, R., Jungreis, I., Loveland,
1317 J., Mudge, J.M., Sisu, C., Wright, J., Armstrong, J., et al. (2018). GENCODE
1318 reference annotation for the human and mouse genomes. *Nucleic Acids*
1319 *Research* 47, D766-D773. 10.1093/nar/gky955.
- 1320 90. Dobin, A., Davis, C.A., Schlesinger, F., Drenkow, J., Zaleski, C., Jha, S., Batut,
1321 P., Chaisson, M., and Gingeras, T.R. (2012). STAR: ultrafast universal RNA-seq
1322 aligner. *Bioinformatics* 29, 15-21. 10.1093/bioinformatics/bts635.
- 1323 91. Love, M.I., Huber, W., and Anders, S. (2014). Moderated estimation of fold
1324 change and dispersion for RNA-seq data with DESeq2. *Genome Biology* 15, 550.
1325 10.1186/s13059-014-0550-8.
- 1326 92. Ritchie, M.E., Phipson, B., Wu, D., Hu, Y., Law, C.W., Shi, W., and Smyth, G.K.
1327 (2015). limma powers differential expression analyses for RNA-sequencing and
1328 microarray studies. *Nucleic Acids Research* 43, e47-e47. 10.1093/nar/gkv007.

- 1329 93. Macchietto, M.G., Langlois, R.A., and Shen, S.S. (2020). Virus-induced
1330 transposable element expression up-regulation in human and mouse host cells.
1331 *Life Sci Alliance* 3. 10.26508/lsa.201900536.
- 1332 94. Shabalin, A.A. (2012). Matrix eQTL: ultra fast eQTL analysis via large matrix
1333 operations. *Bioinformatics* 28, 1353-1358. 10.1093/bioinformatics/bts163.
- 1334 95. Wang, T., Peng, Q., Liu, B., Liu, X., Liu, Y., Peng, J., and Wang, Y. (2020).
1335 eQTLMAPT: Fast and Accurate eQTL Mediation Analysis With Efficient
1336 Permutation Testing Approaches. *Frontiers in Genetics* 10.
1337 10.3389/fgene.2019.01309.
- 1338 96. Wu, T., Hu, E., Xu, S., Chen, M., Guo, P., Dai, Z., Feng, T., Zhou, L., Tang, W.,
1339 Zhan, L., et al. (2021). clusterProfiler 4.0: A universal enrichment tool for
1340 interpreting omics data. *The Innovation* 2, 100141.
1341 <https://doi.org/10.1016/j.xinn.2021.100141>.
- 1342 97. Ghoussaini, M., Mountjoy, E., Carmona, M., Peat, G., Schmidt, E.M., Hercules,
1343 A., Fumis, L., Miranda, A., Carvalho-Silva, D., Buniello, A., et al. (2021). Open
1344 Targets Genetics: systematic identification of trait-associated genes using large-
1345 scale genetics and functional genomics. *Nucleic Acids Res* 49, D1311-d1320.
1346 10.1093/nar/gkaa840.
- 1347 98. Kim, S.-S., Hudgins, A.D., Gonzalez, B., Milman, S., Barzilai, N., Vijg, J., Tu, Z.,
1348 and Suh, Y. (2021). A Compendium of Age-Related PheWAS and GWAS Traits
1349 for Human Genetic Association Studies, Their Networks and Genetic
1350 Correlations. *Frontiers in Genetics* 12. 10.3389/fgene.2021.680560.
1351
1352

1353 **Legends to Figures**

1354

1355 **Figure 1. Overview of the pipeline developed to scan for L1 transcriptional**
1356 **regulators *in silico*.**

1357 **(A)** An illustration of the samples and “omic” data used in this study. Of the 358
1358 European individuals, 187 were female and 171 were male. Of the 86 African
1359 individuals, 49 were female and 37 were male. (Note that Utah subjects are of Northern
1360 European ancestry, and thus part of the European cohort for analytical purposes). **(B)** A
1361 schematic illustrating how genetic variants, gene expression, and TE expression can be
1362 integrated to identify highly correlated SNV-Gene-TE trios. **(C)** A Manhattan plot for the
1363 L1 subfamily *trans*-eQTL analysis in the European cohort. The genes that passed our
1364 three-part integration approach are listed next to the most significant *trans*-eQTL SNV
1365 they were associated with in *cis*. The dashed line at $p = 3.44E-8$ corresponds to an
1366 average empirical FDR < 0.05 , based on 20 random permutations. One such
1367 permutation is illustrated in the bottom panel. The solid line at $p = 2.31E-8$ corresponds
1368 to a Benjamini-Hochberg FDR < 0.05 . The stricter of the two thresholds, $p = 2.31E-8$,
1369 was used to define significant *trans*-eQTLs. FDR: False Discovery Rate. Some panels
1370 were created with BioRender.com.

1371

1372 **Figure 2. Identification of 1st tier candidate L1 expression regulators in the**
1373 **European cohort.**

1374 **(A)** A schematic for how 1st tier candidate genes were defined. In short, these were
1375 genes in trios with index SNVs that were at the top of their respective peak. **(B)** The
1376 three-part integration results for three protein-coding genes—*STARD5*, *IL16*,
1377 *HSD17B12*—that we considered first tier candidates for functional, *in vitro* testing. In the
1378 left column are the *trans*-eQTLs, in the middle column are the *cis*-eQTLs, and in the
1379 right column are the linear regressions for gene expression against L1 subfamily
1380 expression. Expression values following an inverse normal transform (INT) are shown.
1381 The FDR for each analysis is listed at the top of each plot. FDR: False Discovery Rate.

1382

1383 **Figure 3. L1 *trans*-eQTLs are associated with subtle, widespread differences in TE**
1384 **families and known TE-associated pathways.**

1385 **(A)** Scheme for functionally annotating gene-linked index SNVs by GSEA. **(B)** GSEA
1386 analysis for shared, significantly regulated TE family gene sets across genotypes for
1387 rs11635336 (*IL16/STARD5*), rs9271894 (*HLA*), and rs1061810 (*HSD17B12*). **(C)** GSEA
1388 plots for the L1 family gene set results summarized in **(B)**. For these plots, the FDR
1389 value is listed. GSEA analysis for top, shared, concomitantly regulated **(D)** MSigDB
1390 Hallmark pathway, **(E)** GO Biological Process, and **(F)** Reactome pathway gene sets
1391 across genotypes for rs11635336 (*IL16/STARD5*), rs9271894 (*HLA*), and rs1061810
1392 (*HSD17B12*). Shared gene sets were ranked by combining p-values from each
1393 individual SNV analysis using Fisher's method. In each bubble plot, the size of the dot
1394 represents the $-\log_{10}(\text{FDR})$ and the color reflects the normalized enrichment score.
1395 FDR: False Discovery Rate.

1396

1397 **Figure 4. Impact of *IL16* and *STARD5* overexpression on LCL gene and TE**
1398 **expression landscapes.**

1399 *IL16* and *STARD5* overexpression induce changes consistent with their known biology,
1400 as well as subtle but widespread upregulation of TE families. **(A)** Scheme for
1401 experimentally validating the roles of *IL16* and *STARD5* in L1 regulation. GSEA analysis
1402 for top, differentially regulated **(B)** GO Biological Process and **(C)** Reactome pathway
1403 gene sets following *IL16* overexpression. GSEA analysis for top, differentially regulated
1404 **(D)** GO Biological Process and **(E)** Reactome pathway gene sets following *STARD5*
1405 overexpression. **(F)** GSEA analysis for shared, significantly regulated TE family gene
1406 sets following *IL16* and *STARD5* overexpression. **(G)** GSEA plots for the L1 family gene
1407 set results summarized in **(F)**. For these plots, the FDR value is listed. In each bubble
1408 plot, the size of the dot represents the $-\log_{10}(\text{FDR})$ and the color reflects the normalized
1409 enrichment score. FDR: False Discovery Rate. Some panels were created with
1410 BioRender.com.

1411

1412 **Figure 5. rhIL16 treatment is sufficient to transiently upregulate an L1 family gene**
1413 **set.**

1414 **(A)** Scheme for experimentally validating the role of rhIL16 in L1 regulation. GSEA
1415 analysis for top, shared, concomitantly regulated **(B)** GO Biological Process and **(C)**
1416 Reactome pathway gene sets following *IL16* overexpression and rhIL16 exposure for 24
1417 hours. Shared gene sets were ranked by combining p-values from each individual
1418 treatment analysis using Fisher's method. **(D)** GSEA analysis for top, differentially
1419 regulated TE family gene sets following rhIL16 exposure for 24 hours. The GSEA plot
1420 for the L1 family gene set result summarized in the bubble plot is also shown. For this
1421 plot, the FDR value is listed. In each bubble plot, the size of the dot represents the -
1422 $\log_{10}(\text{FDR})$ and the color reflects the normalized enrichment score. FDR: False
1423 Discovery Rate. Some panels were created with BioRender.com.

1424

1425 **Figure 6. Consistent cellular responses to *IL16* overexpression, *STARD5***
1426 **overexpression, and rhIL16 exposure for 24 hours.**

1427 *IL16* overexpression, *STARD5* overexpression, and rhIL16 exposure for 24 hours are
1428 associated with subtle but widespread differences in TE families and known TE-
1429 associated pathways. **(A)** Scheme for assessing concordantly regulated TE family and
1430 pathway gene sets across conditions where an L1 gene set is upregulated. GSEA
1431 analysis for top, shared, concomitantly regulated **(B)** TE family, **(C)** MSigDB Hallmark
1432 pathway, **(D)** GO Biological Process, and **(E)** Reactome pathway gene sets following
1433 *IL16* overexpression, *STARD5* overexpression, and rhIL16 exposure for 24 hours.
1434 Shared gene sets were ranked by combining p-values from each individual treatment
1435 analysis using Fisher's method. In each bubble plot, the size of the dot represents the -
1436 $\log_{10}(\text{FDR})$ and the color reflects the normalized enrichment score. FDR: False
1437 Discovery Rate.

1438

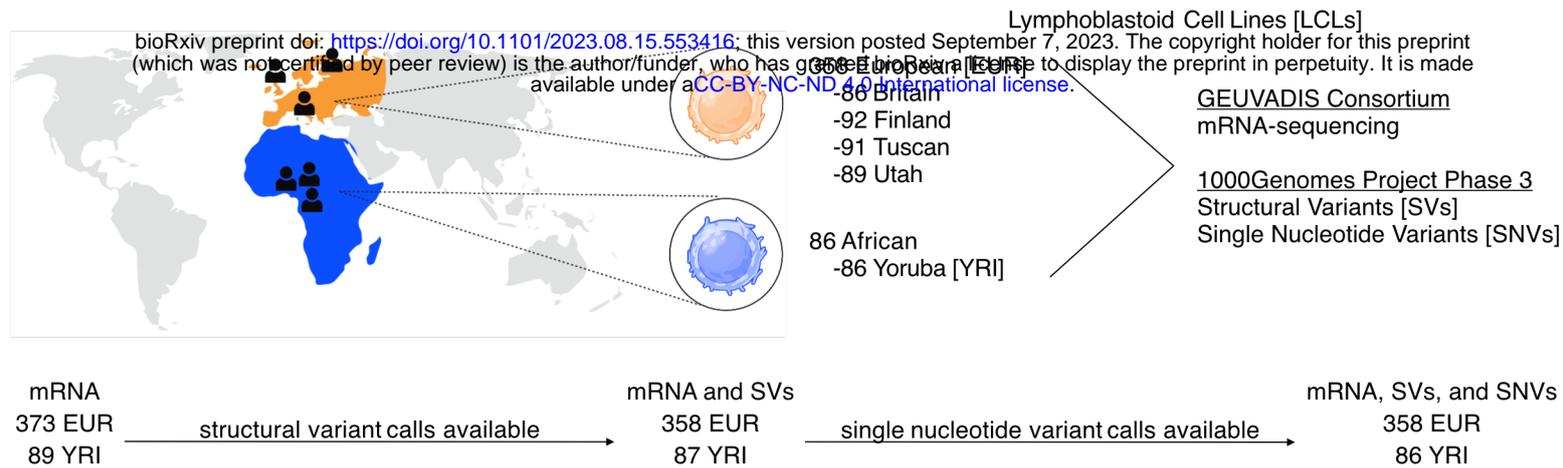
1439 **Figure 7. L1 *trans*-eQTLs are co-associated with aging traits in GWAS databases.**

1440 **(A)** Scheme for obtaining *trans*-eQTL SNV-associated aging phenotypes from the Open
1441 Targets Genetics platform. **(B)** A pie chart representing the number of SNVs (222/499)
1442 associated with an aging-related MeSH trait, either by PheWAS or indirectly linked to
1443 the phenotype through a proxy lead SNP in LD with the SNV. **(C)** Histogram depicting
1444 the distribution of number of aging MeSH traits associated with the 222/499 SNVs by

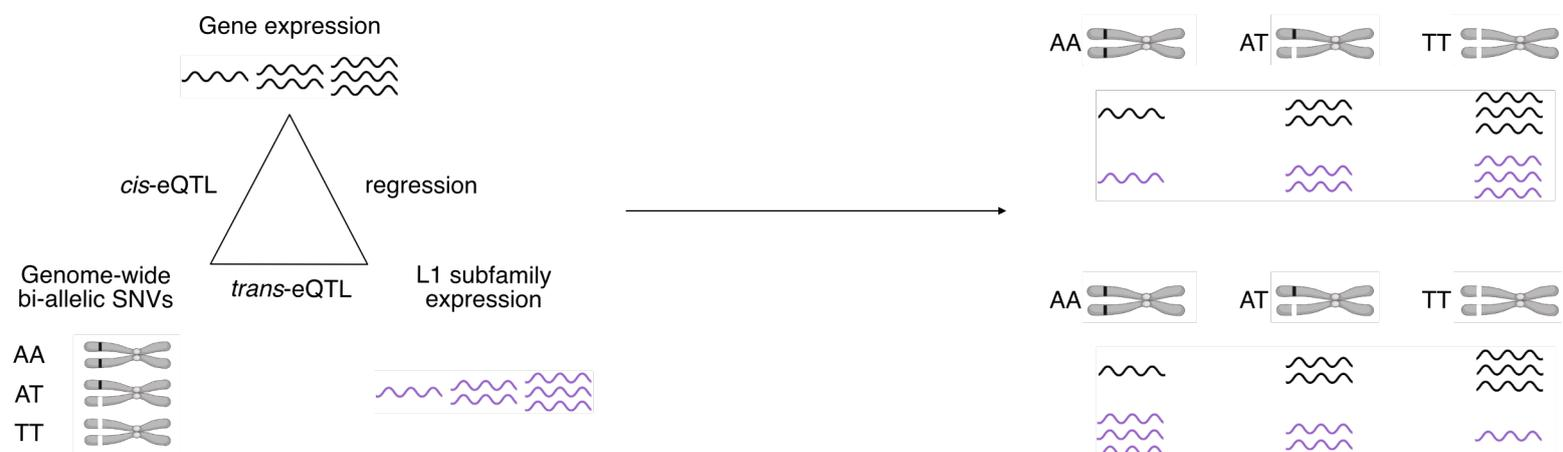
1445 PheWAS. **(D)** Histogram depicting the distribution of number of aging MeSH traits linked
1446 with the 222/499 SNVs through a proxy lead SNP in LD with the SNVs. **(E)** A diagram
1447 highlighting the organ targets of the top 10 most frequently associated aging traits. **(F)**
1448 The concentrations of circulating IL16 in aging mice of both sexes was assessed by
1449 ELISA. Significance across age in each sex was assessed using a Wilcoxon test. The
1450 p-values from each sex (females in pink and males in blue) were combined by meta-
1451 analysis using Fisher's method. Any p-value < 0.05 was considered significant. Some
1452 panels were created with BioRender.com.
1453
1454

Figure 1

A Samples and data used in this study



B Scheme for *in silico* identification of candidate transposon-subfamily regulators



C Manhattan plots for European L1 *trans*-eQTL analysis

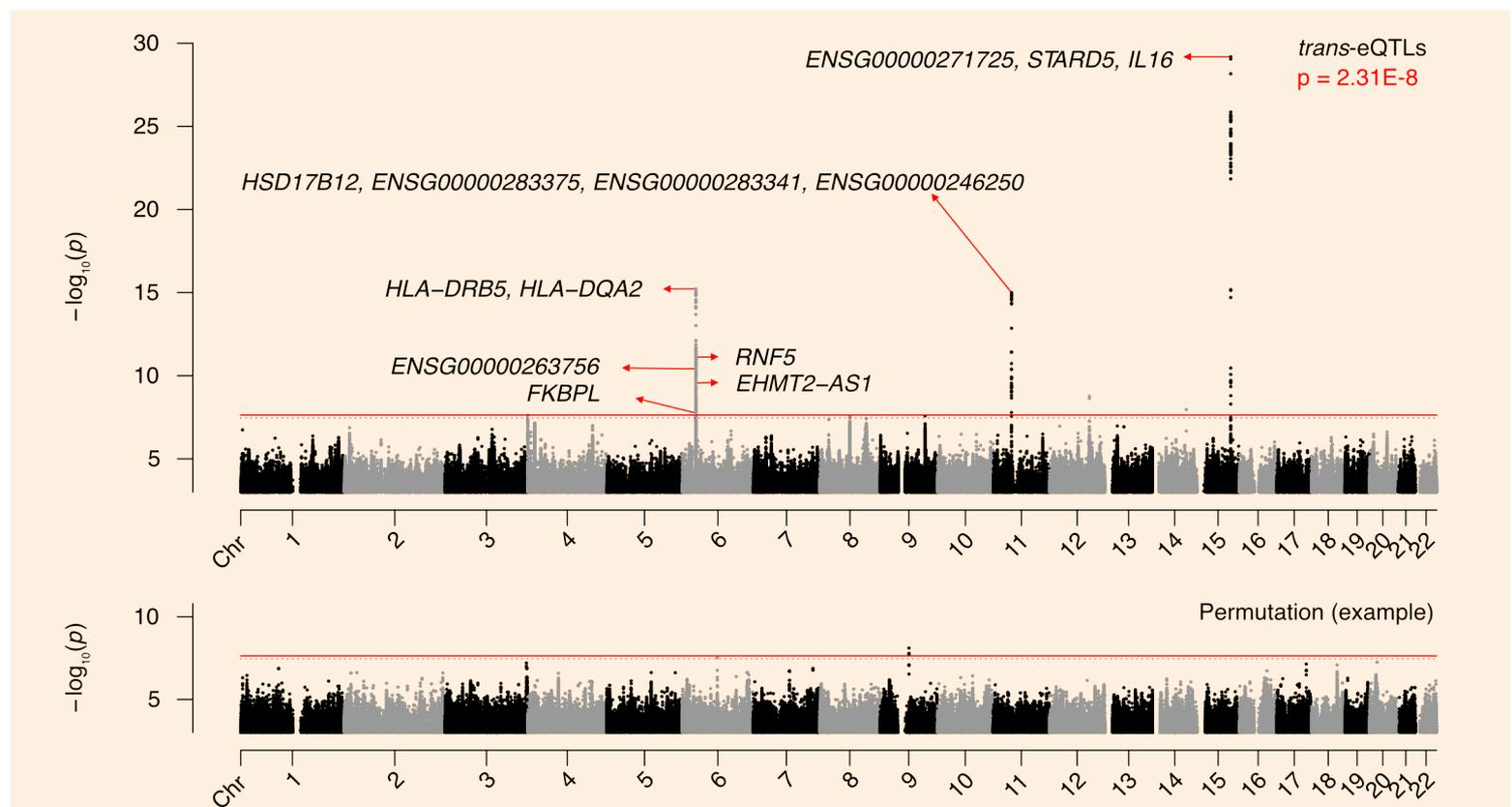
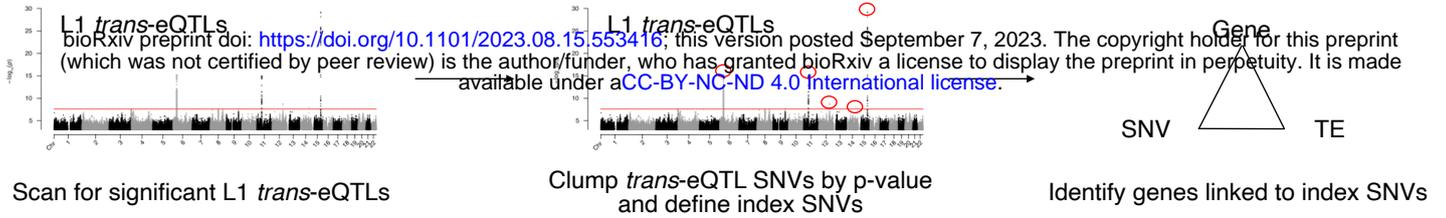


Figure 2

A Scheme for defining 1st tier candidate genes



B *In silico* screen results for 1st tier candidate regulators

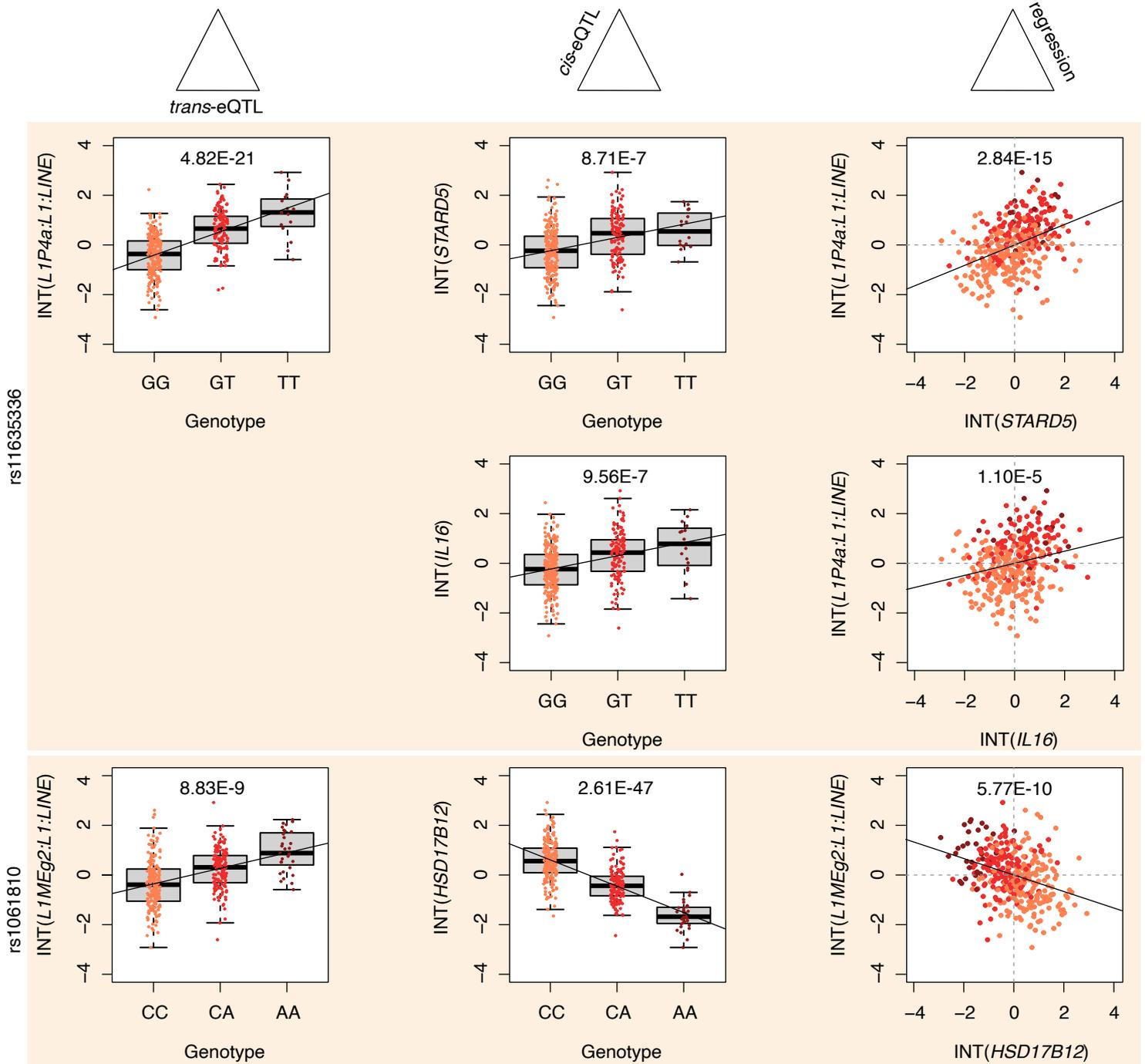
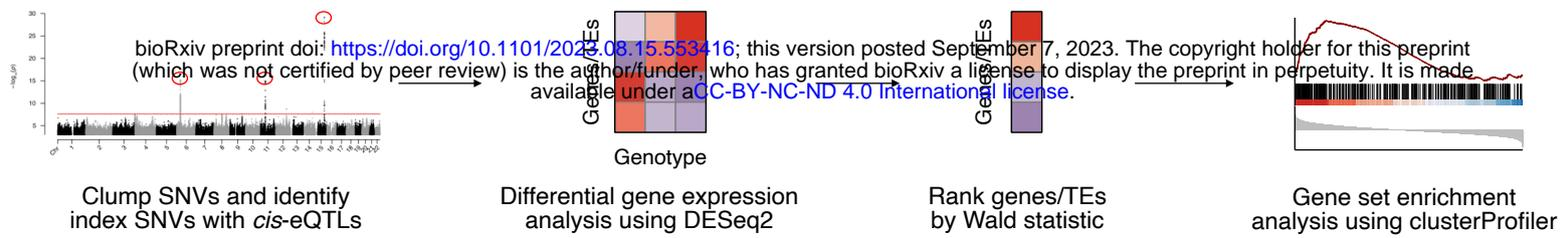
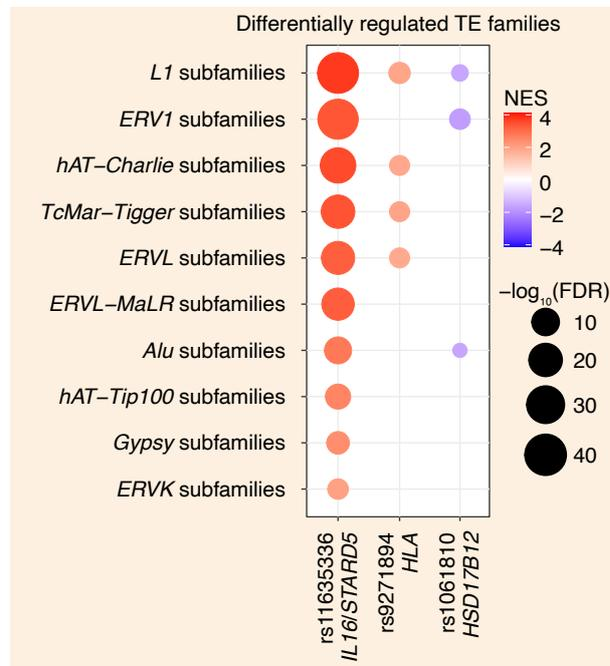


Figure 3

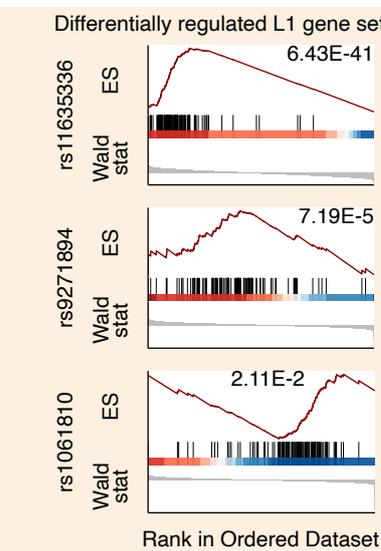
A Scheme for functionally annotating SNVs



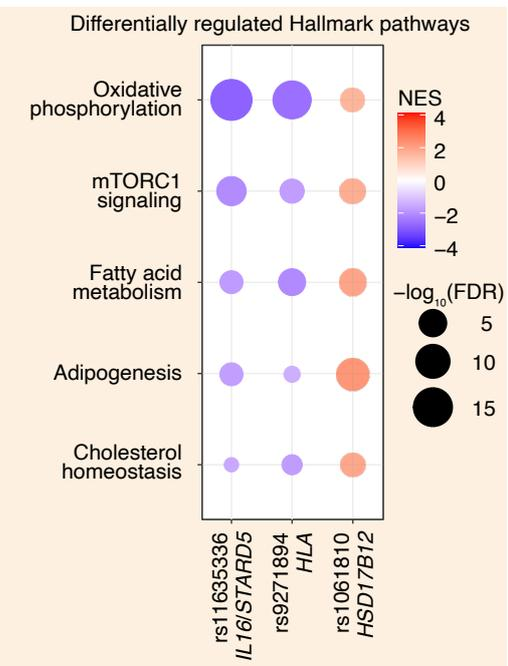
B Index SNV associations with TE family gene sets



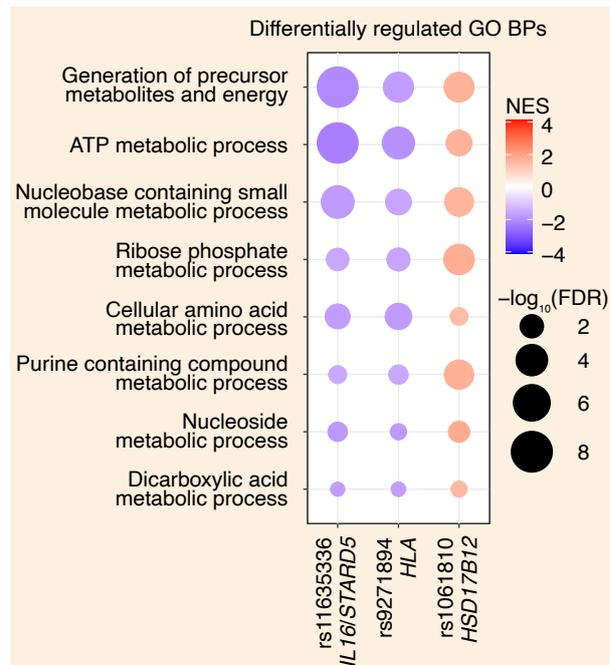
C Index SNV associations with an L1 family gene set



D Index SNV associations with MSigDB Hallmark gene sets



E Index SNV associations with GO Biological Process gene sets



F Index SNV associations with Reactome gene sets

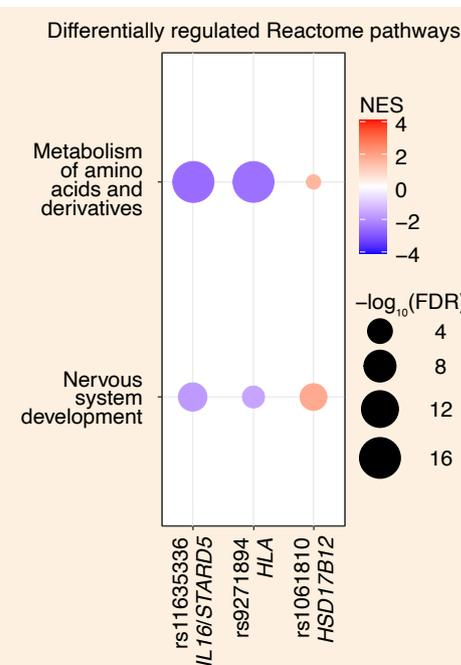
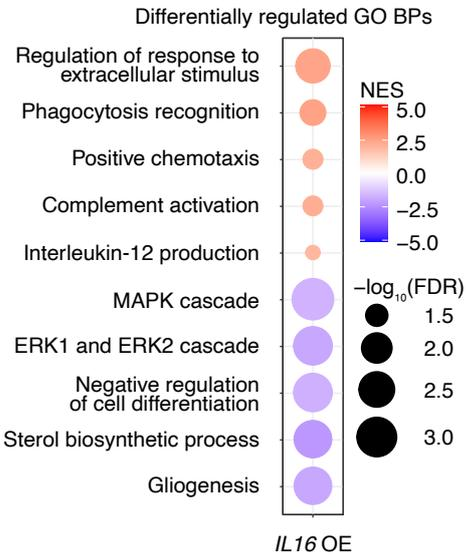


Figure 4

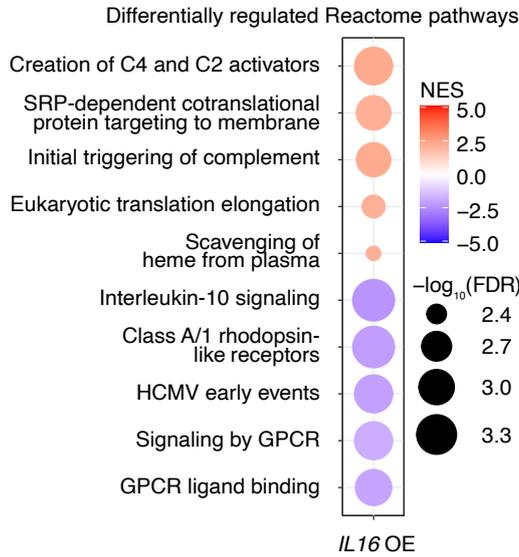
A Scheme for assessing the effects of candidate genes on L1 expression



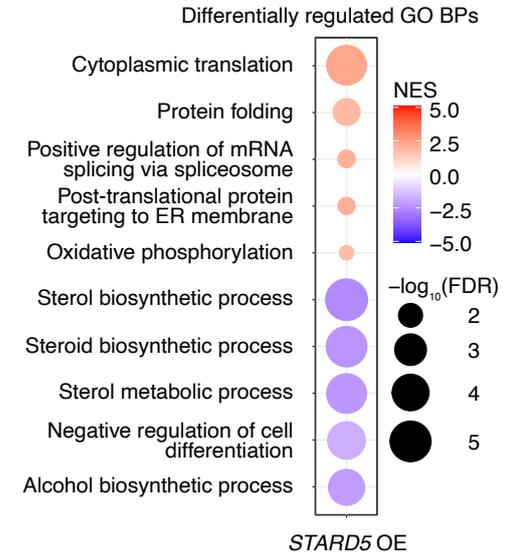
B Top enriched GO Biological Processes following *IL16* overexpression



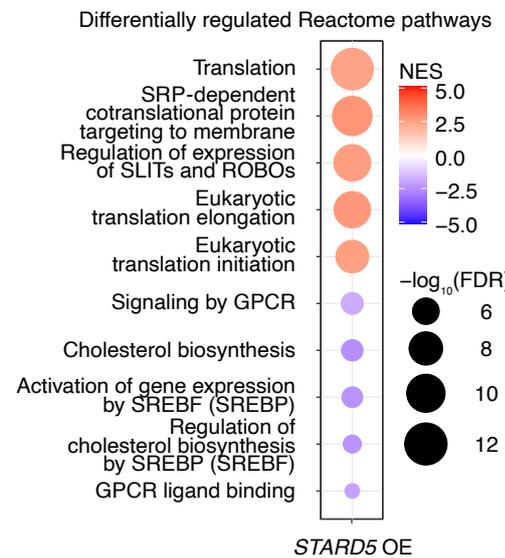
C Top enriched Reactome gene sets following *IL16* overexpression



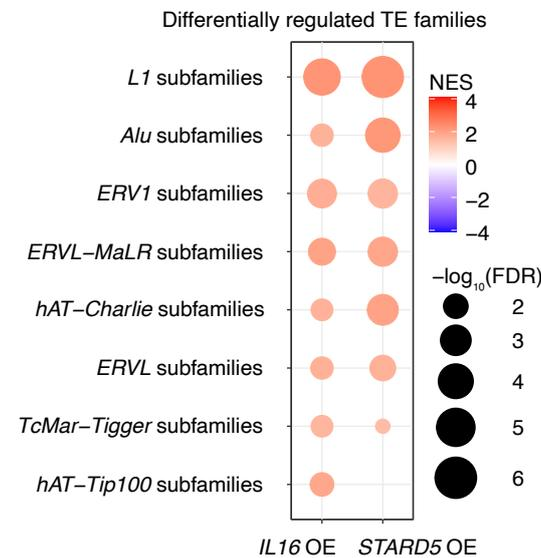
D Top enriched GO Biological Processes following *STARD5* overexpression



E Top enriched Reactome gene sets following *STARD5* overexpression



F *IL16* and *STARD5* associations with TE family gene sets



G *IL16* and *STARD5* associations with an L1 family gene set

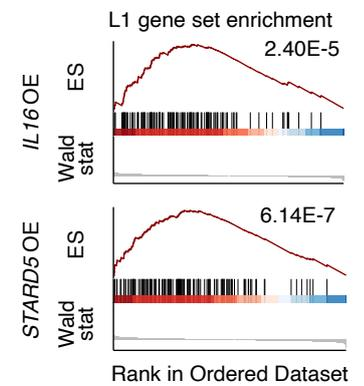
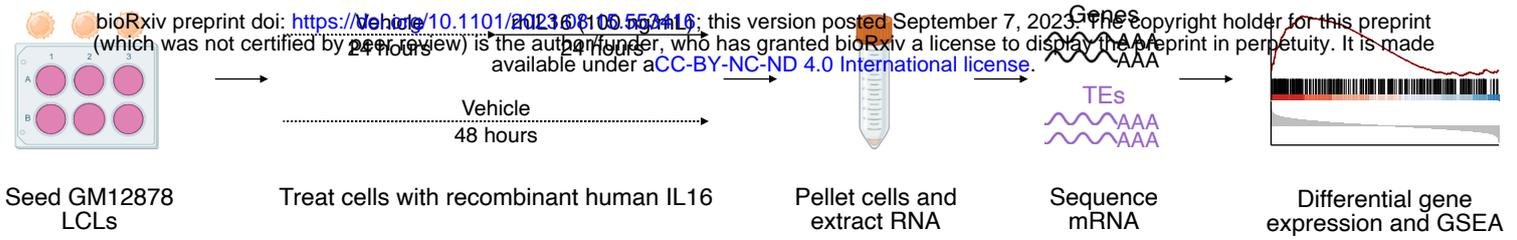
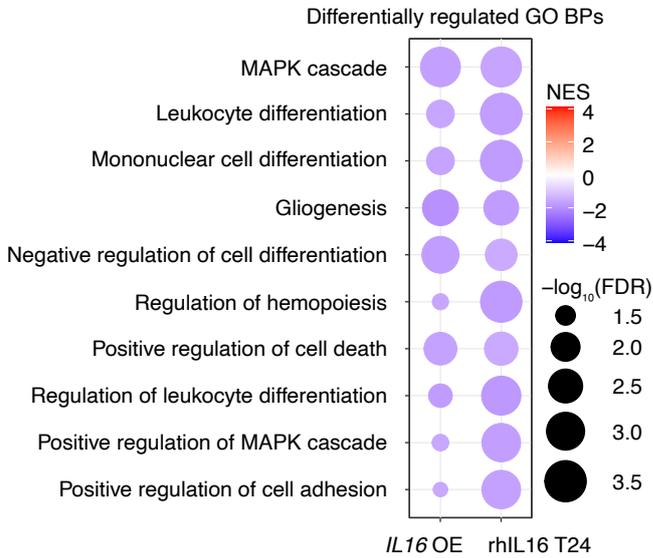


Figure 5

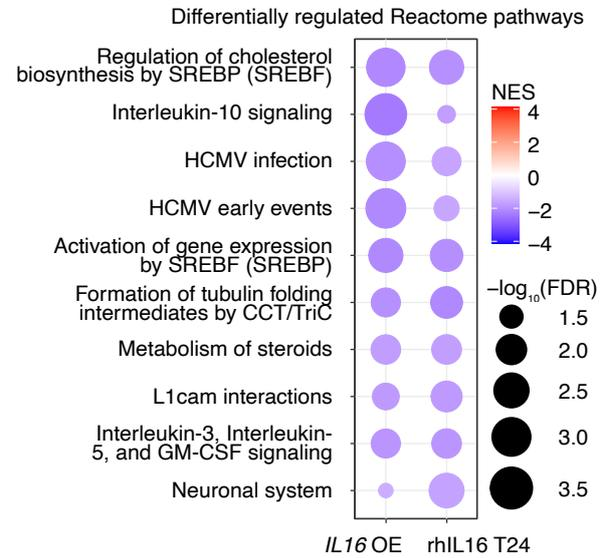
A Scheme for assessing the effects of IL16 protein on L1 expression



B Top shared GO Biological Processes



C Top shared Reactome gene sets



D rhIL16 associations with TE family gene sets

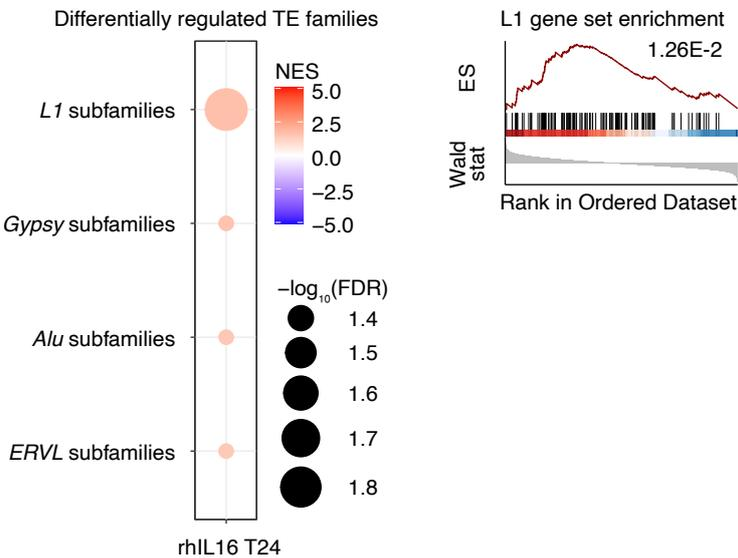


Figure 6

A Scheme for assessing shared pathway changes in conditions with L1 regulation

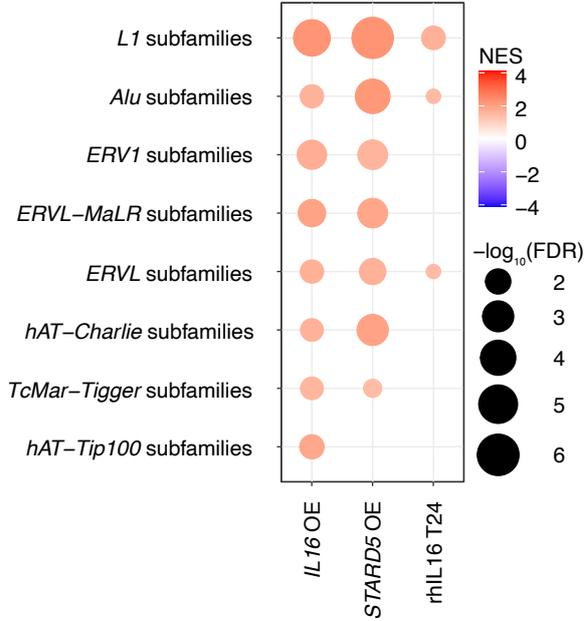


GSEA for experimental conditions with L1 regulation

Identify common pathways

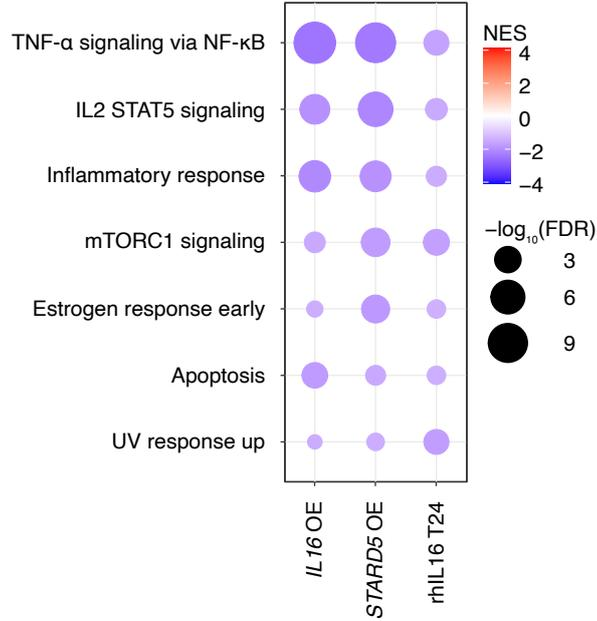
B Shared upregulated TE family gene sets

Differentially regulated TE families



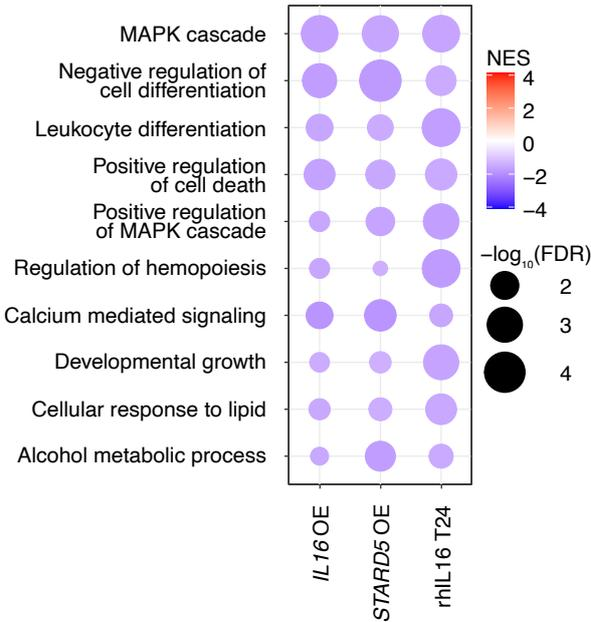
C Top shared Hallmark pathways

Differentially regulated Hallmark pathways



D Top shared GO Biological Processes

Differentially regulated GO BPs



E Top shared Reactome pathways

Differentially regulated Reactome pathways

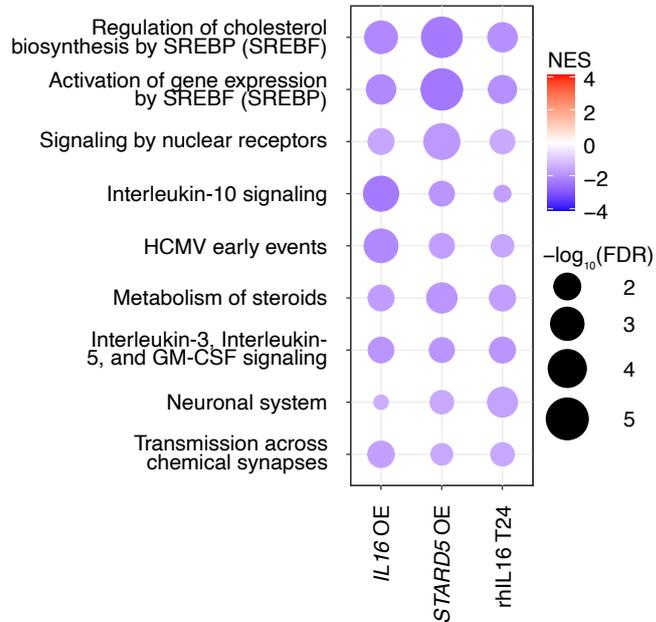
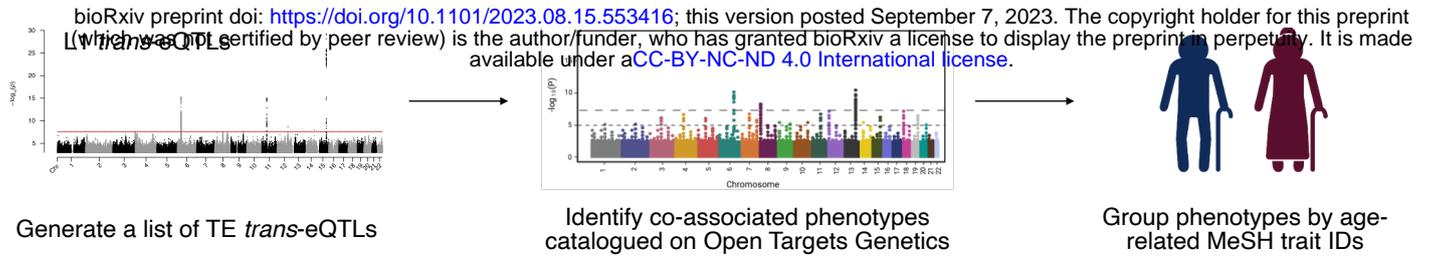
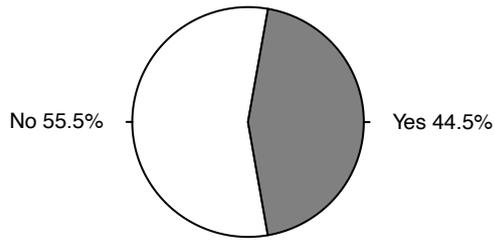


Figure 7

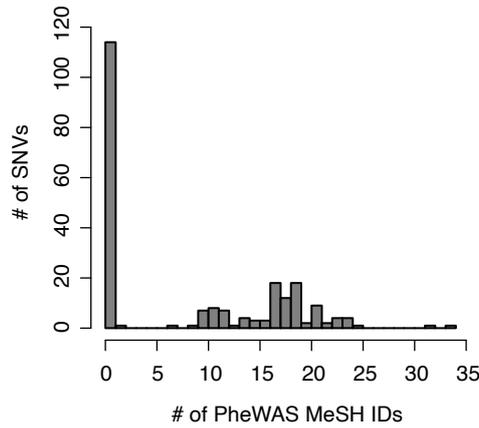
A Scheme for identifying TE eQTL co-associated aging traits



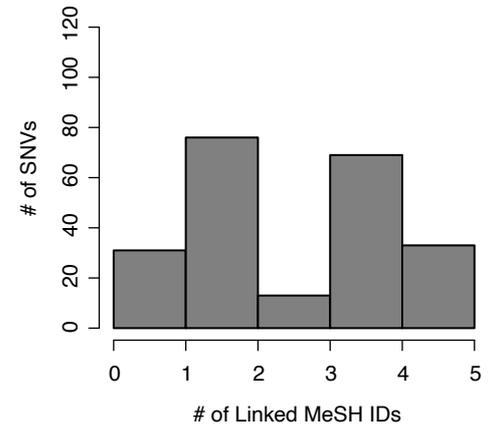
B Number of SNVs with an age-related MeSH trait



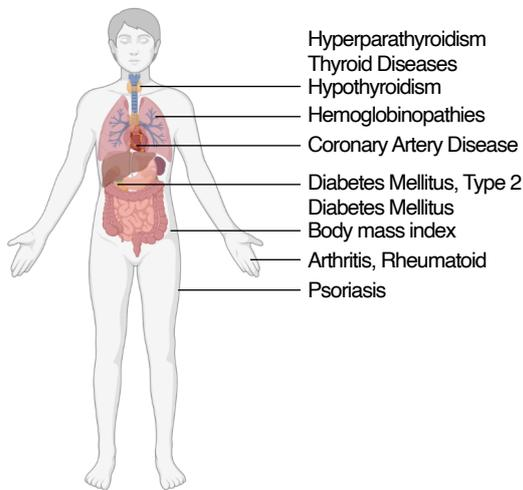
C Number of associated age-related traits per SNV



D Number of linked age-related traits per SNV



E Top traits with the most number of associated SNVs



F Mouse serum [IL16] with age

